International Journal of Pharmaceutics 698 (2026) 126885

Contents lists available at ScienceDirect

International Journal of Pharmaceutics

journal homepage: www.elsevier.com/locate/ijpharm

Nanostructured lipid carrier enabled delivery of levofloxacin and clove essential oil to overcome *Pseudomonas aeruginosa* biofilm infection in burn wounds- a synergistic approach

Karan Razdan [a,b], Matthew Allott [c], Shashi Kanta [d], Ekta Chaudhary [d], Deepak Kumar Rahi [d], Seema Kumari [d], Tamara Zwain [b], Jorge Garcia Lara [c,e], Vivek Ranjan Sinha [a,*], Kamalinder K. Singh [b,e,**]

[a] Pharmaceutics Division, University Institute of Pharmaceutical Sciences, UGC-Centre of Advanced Study, Panjab University, Chandigarh, India
[b] School of Pharmacy and Biomedical Sciences, University of Lancashire, Preston PR1 2HE, United Kingdom
[c] School of Medicine and Dentistry, University of Lancashire, Preston PR1 2HE, United Kingdom
[d] Department of Microbiology, Basic Medical Sciences, Panjab University, Chandigarh, India
[e] Biomedical Evidence Based Transdisciplinary (BEST) Health Research Institute, University of Lancashire, Preston PR1 2HE, United Kingdom

ARTICLE INFO

Keywords:
Antibiofilm
Chronic wound
Clove oil
Hydrogel
Levofloxacin
Nanostructured lipid carriers
P. aeruginosa

ABSTRACT

Conventional antibiotics struggle to completely eradicate the infection because of their ineffective penetration of biofilms. New multimodal strategy integrating antibiofilm agent with antimicrobials delivered as nanomedicine could be a powerful approach to overcome biofilm resistance. Bioactive essential oils have recently garnered great attention because of their biofilm disruption and antibiofilm activity. The present study developed an integrated functional nanostructured lipid carrier (NLCs) combining clove essential oil (CO) and levofloxacin (LFX) as model antibiotic for localized delivery as hydrogel for treatment of burn wounds infected with *P. aeruginosa* biofilms. *In vitro* cell line studies demonstrated concentration dependent uptake of LFX-CO-NLCs in human dermal fibroblasts and normal human epithelial keratinocytes, and exhibhited cytocompatibility and fibroblast migration in scratch wound assay. Crystal violet assay validated strong antibiofilm effect of LFX-CO-NLCs. The nanoparticles were able to infiltrate through *P. aeruginosa* biofilm and be up taken by bacterial cells as evidenced by confocal microscopy. LFX-CO-NLCs hydrogel showed appreciable textural profile and pseudoplastic behavior which facilitated topical application. *In vivo* burn wound in mice with *P. aeruginosa* infection displayed early wound closure, significantly improved infection clearance and enhanced collagen deposition and wound healing after treatment with LFX-CO-NLCs hydrogel in comparison to other treatment groups. Wounds were found to be devoid of any bacterial presence after 7 days of LFX-CO-NLCs hydrogel application. It is propounded that this industrially viable technology holds great promise as future therapeutics for chronic wound infections.

1. Introduction

Antimicrobial resistance (AMR) is an alarming issue affecting worldwide public health and necessitates quick and drastic action from all governmental entities and society (Podolsky, 2018). It has been predicted by the World Health Organization (WHO) that by the year 2050, antibiotic resistance could lead to 10 million fatalities annually (Henostroza et al., 2022). The formation of bacterial biofilms significantly contributes to the emergence of AMR and adds further complexity to this problem. Once bacteria adhere to any biotic/abiotic surface, they start producing extracellular polymeric substances (EPS) as an adaptive response to get enmeshed within the matrix which serves as their protective shield. Wound bed creates a conducive environment for the development of bacterial biofilm, primarily attributable to the presence of necrotic tissue. The structural framework of wound debris and EPS together create a physical barrier that prevents the invasion of fibroblasts, keratinocytes, and immune cells. Due to attachment to the matrix, antibiotics are unable to reach adequate concentration in the

* Corresponding author.
** Corresponding author at: School of Pharmacy and Biomedical Sciences, University of Lancashire, Preston PR1 2HE, United Kingdom
E-mail addresses: vrsinha@pu.ac.in (V.R. Sinha), ksingh1@lancashire.ac.uk (K.K. Singh).

https://doi.org/10.1016/j.ijpharm.2026.126885
Received 7 February 2026; Received in revised form 23 March 2026; Accepted 13 April 2026
Available online 17 April 2026

wound bed which breeds resistance (Ciofu et al., 2022). Moreover, bacteria residing within the biofilms can demonstrate resistance to conventional antimicrobial treatments that is up to a thousand folds greater than that of their planktonic form (Uruén et al., 2020).

Burn injuries compromise the integrity of the skin barrier, rendering individuals susceptible to opportunistic infections. Among the primary infectious agents that colonize burn wounds is *Pseudomonas aeruginosa*, which can lead to significant infections by employing biofilm formation as a strategy to evade both the immune response and antibiotic therapies (Sathe et al., 2023). A recent investigation conducted by Ghasemian et al. revealed that forty isolates of *P. aeruginosa*, sourced from patients with burn wounds, exhibited significant biofilm production capabilities (Ghasemian et al., 2023). The presence of biofilm formation and various virulence factors, coupled with antibiotic resistance, constrains the effective treatment by conventional antibiotics available for infections associated with burn wounds (Ciofu et al., 2022; Uruén et al., 2020).

Given the strong contribution of biofilms towards the development of AMR and persistence of infection, delivery of an integrated dual nano-system (NS) combining an antibiofilm agent with an antibiotic can be a powerful strategy to provide a synergistic effect and clearance of infection from the wounds and prevent AMR (Razdan et al., 2022). NS can disrupt the growth of bacterial biofilms via physical damage, oxidative stress, and thermal injury mechanisms, thereby increasing the ability of an antibiotic to penetrate biofilms, enable targeted delivery and intracellular killing of bacteria (Diab et al., 2015). In this context, nanostructured lipid carriers (NLCs) are an excellent nano-system choice as they outperform alternative colloidal nanoparticulate delivery systems in terms of drug loading, release rate, bioavailability, stability, scalability and their suitability for topical delivery (Üner, 2006; Elmowafy and Al-Sanea, 2021). NLCs are designed using solid and liquid lipids which are biocompatible and biodegradable. Low index of crystallinity of the lipid blend in NLCs prevent drug expulsion which is usually observed with solid lipid nanoparticles (SLNs) (Üner, 2006).

Bioactive essential oils (EOs) have been documented to exhibit multiple functions, including ability to disrupt biofilm formation and antibacterial activity (Budzyńska et al., 2011; Bazargani and Rohloff, 2016). Among various EOs, numerous literature findings have reported clove oil (CO) to possess excellent antibacterial and antibiofilm properties owing to the presence of its major component, eugenol. Clove oil primarily impacts the structural integrity and functional capabilities of the cell membrane by disrupting its fluidity and permeability as well as impairing the functioning of membrane transport proteins. The biofilm's dense membrane structure can be compromised, inhibiting the secretion of extracellular polysaccharides and proteins (Elbestawy et al., 2023; Manzoor et al., 2023). Moreover, due to its antioxidant and anti-inflammatory characteristics, CO has shown potential in promoting wound healing (Hameed et al., 2021; Banerjee et al., 2020). Additionally, clove oil has been designated GRAS (generally regarded as safe) status by US-FDA thus making it safe for topical application. In this study, CO was selected as biofilm disruptor as well as utilized as bioactive liquid lipid to form functional NLCs.

Levofloxacin (LFX), a prominent member of the fluoroquinolone class of antibiotics, utilized extensively for its broad-spectrum activity was used as a model antibiotic to be incorporated in the functional NLCs. LFX is administered orally to address both complicated and uncomplicated infections of the skin and its associated structures (Giordano et al., 2007). However, oral administration of the antibiotic leads to side-effects such as nausea, gastrointestinal disturbances and tendon rupture (Liu, 2010). LFX has been reported to be used in various wound dressings for treatment of infected wounds (Valizadeh et al., 2021; Pásztor et al., 2017; Siafaka et al., 2016). Hence, topical treatment of infected wounds would be beneficial by circumventing the side-effects and provide high local concentration of antibiotic at the wound site. Moreover, combining LFX with CO in the NLCs would enhance its penetration in the biofilm and eradicate infection. Nanoparticles enhance biofilm penetration by virtue of their small size, enabling diffusion into EPS matrix and migrate into the biofilm. The penetration may depend on the biofilm charge, pore size, hydrophobicity, and chemical gradient of EPS (Alhariri et al., 2017; Zou et al., 2022).

The present research reports a multimodal NLC system where CO performs dual role of liquid lipid in the NLCs as well as a biofilm disruptor. The integrated NLC system (LFX-CO-NLCs) co-loaded with LFX and CO enhanced penetration and eradication of *P. aeruginosa* biofilm to clear the infection from the burn wounds. Interestingly, the incorporation of CO in the NLCs as a bioactive liquid lipid also enhanced the drug loading of LFX while simultaneously reducing its volatility and oxidative degradation and retaining its biological activity thus, alleviating the limitations associated with other nanocarriers (Ghodrati et al., 2019; Sepahvand et al., 2022). The work encompasses development, optimization and detailed characterization of LFX-CO-NLCs and its hydrogel. *In-vitro* cell culture studies emphasized the cellular compatibility, cell uptake and mechanism of cell uptake in normal human keratinocytes and human dermal fibroblast cells.

In-vitro penetration into biofilms and anti-biofilm effect were demonstrated through scanning electron microscopy (SEM), fluorescence microscopy, crystal violet assay and live/dead cell staining in *P. aeruginosa* biofilm cultures, while *in vivo* efficacy was established in burn wound infected with *P. aeruginosa* biofilm in mice. To the best of our knowledge this is the first report of integrated NLCs hydrogel system co-loaded with LFX and CO and their subsequent detailed physicochemical, microbiological and biological evaluation. It is contemplated that this commercially viable dual functional NS can be a future therapeutic for *P. aeruginosa* wound infections.

2. Materials and methods

All chemicals, reagents, culture medium, bacterial strains, cell lines used in the study are described in supplementary material S1.

2.1. Selection of solid lipid and liquid oil phase

Appropriate selection of solid lipid was made by determining the solubility of LFX in various lipids (Precirol ATO5, Dynasan 114, Compritol 888 ATO, stearic acid, Imwitor 900K and glyceryl monostearate). Briefly, LFX was added in increments to 1 g of lipid and heated in a water bath at 70–80°C. The mixture was visually observed for LFX solubilization (Sakellari et al., 2021). Clove oil was selected as liquid oil phase for NLCs preparation based on its reported antibiofilm and drug solubilizing properties for LFX (Razdan et al., 2022).

2.2. Preparation and physicochemical characterizations of co-loaded NLCs (LFX-CO-NLCs)

LFX-CO-NLCs were fabricated using hot emulsification followed by ultrasonication method. Briefly, after melting the solid lipid (3–5% w/w) at a temperature of 70°C, clove oil (3–5%) and surfactants (2–4.5%) were added. LFX was added in various concentrations (0.25–1% w/w) to the lipid mix and mixed at 1000 rpm for 5 min. Aqueous phase heated at 70°C containing sodium cholate was transferred to lipid phase under magnetic mixing. The pre-emulsion was sonicated using a probe sonicator (Vibra Cell Sonics, USA) for 3 min at 40% amplitude and allowed to cool to obtain the NLCs. The schematic illustration of prepartion of LFX-CO-NLCs is given in Fig. 1A.

Clove oil loaded NLCs (CO-NLCs), which did not include LFX, were prepared using the same procedure while rhodamine 123 (R123)-labeled NLCs (R-LFX-CO-NLCs) were formulated by adding the R123 dye to the melted lipidic phase. The LFX-CO-NLCs were characterized for particle size (PS), polydispersity index (PDI), and zeta potential (ZP), entrapment efficiency, transmission electron microscopy (TEM), Differential Scanning Calorimetry (DSC), Thermogravimetric Analysis (TGA) and Fourier-transform infrared spectroscopy (FTIR) as per the methods given in supplementary material S2. Gas chromatography mass

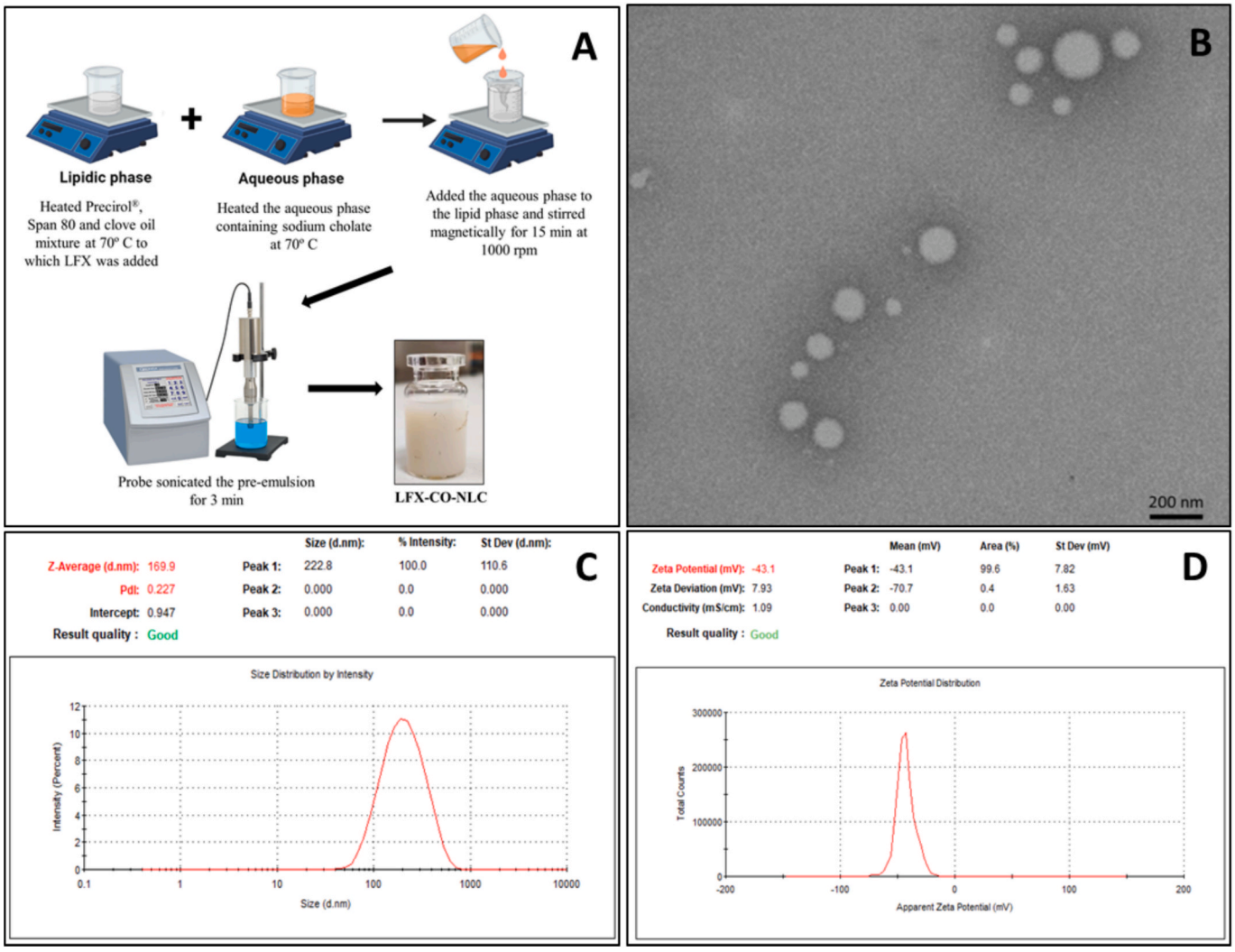

Fig. 1. (A) Schematic illustration of preparation of integrated levofloxacin and clove oil biofunctional nanostructured lipid carriers [LFX-CO-NLCs]. **(B)** TEM photomicrograph, **(C)** Particle size distribution graph by intensity and **(D)** Zeta potential graph for LFX-CO-NLCs.

spectrometry (GCMS) analysis of LFX-CO-NLCs was carried out as per method given in supplementary material S3 and compared with GCMS chromatograph of CO.

2.3. Preparation and characterization of LFX-CO-NLCs hydrogel

To enable localized delivery and enhance retention at the wound site, NLCs were converted into hydrogel by adding hydrophilic polymer Carbopol 934P. Accurately weighed quantities of Carbopol 934P (0.5–2% w/v) were dispersed in LFX-CO-NLCs and allowed to hydrate for at least 12 h after which few drops of triethanolamine were added to neutralize and form hydrogel and the pH was determined. Rheological profile of LFX-CO-NLCs hydrogel was assessed using Rheolab QC rotational rheometer (Anton Paar, Germany) by applying variable shear rate (1–120 s^{-1}) at 25 °C. The Texture Analyzer™ (M/S Stable MicroSystems Ltd., UK) was employed to assess the textural characteristics of the optimized LFX-CO-NLCs hydrogel, specifically focusing on parameters such as firmness, consistency, stickiness, and cohesiveness (Razdan et al., 2023).

2.4. In-vitro drug release

Drug release from LFX-CO-NLCs, plain LFX gel, and LFX-CO-NLCs hydrogel was determined in phosphate-buffered saline (PBS) at pH 7.4, maintained at a temperature of 32 ± 0.5 °C. This assessment utilized a semi-permeable membrane (Himedia; MWCO:12 kDa) clamped into a Franz diffusion cell assembly. Samples were collected over the 8 h period and analyzed using HPLC with a detection wavelength set at 295 nm (Razdan et al., 2023).

2.5. Stability studies

To evaluate the shelf life, LFX-CO-NLCs and LFX-CO-NLCs hydrogel, were stored for a duration of six months at 25°C ± 2°C/60% ± 5% RH and at 40°C ± 2°C/75% ± 5% RH, respectively in accordance with the International Conference on Harmonization (ICH) guidelines, Q1A (R2) and evaluated for physical appearance, pH, and percent drug content for LFX-CO-NLCs hydrogel and PS, PDI and zeta potential for LFX-CO-NLCs, at intervals of 0, 1, 3, and 6 months (Razdan et al., 2023).

2.6. In vitro cell culture studies

2.6.1. Cell culture

NHEK cells were maintained in KGM™ Gold keratinocyte growth medium BulletKit™ (added with gentamycin-amphotericin, hydrocortisone, transferrin, epinephrine, bovine pituitary extract, insulin, and human epidermal growth factor) [Clonetics™, Lonza, Switzerland]. HDF-a cells were cultured in a fibroblast medium supplemented with

fetal bovine serum, fibroblast growth supplement, and penicillin-streptomycin.

2.6.2. Cell-viability assay

The method is elaborated in supplementary information S4.

2.6.3. Cell cycle analysis

Cell cycle analysis of HDF-a cells was performed by utilizing propidium iodide (PI) staining as reported previously (Zwain et al., 2021). Briefly, HDF-a cells were grown in a 12-well plate at a seeding density of $5x10^4$ cells/well for 24 h at 37°C. Following this, the cells were treated with LFX-CO-NLCs, CO-NLCs, and LFX at two different concentrations (1 and 10 μg/ml) and incubated for an additional 24 h. Later, the cells were pelleted and resuspended in 70% ice-cold ethanol for storage at −20°C for 24 h. After washing with PBS and centrifugation, the fixed cells were added to a V-shaped non-tissue culture 96-well plate. The cells were incubated for 2 h following treatment with PI (500 μg/ml stock) and RNAase (10 mg/ml). The distribution of the cell cycle was analyzed using a flow cytometer (Guava, easyCyte HT, Merck, Germany), measuring fluorescence intensity at 488 nm.

2.6.4. Cellular uptake studies

2.6.4.1. Quantitative uptake. For the concentration-dependent quantitative uptake, HDF-a and NHEK cells were cultured in a 12-well plate at densities of 3.6 x 10^4 cells/well and 4 x 10^4 cells/well, respectively, followed by a 24-h incubation. After the incubation, R-LFX-CO-NLCs (0.5, 1, 5, and 10 μg/ml) prepared in fresh medium were introduced into the corresponding wells and incubated for an additional 4 h. Following the incubation, the cells were pelleted using standard procedure and resuspended in 0.25 ml of ice-cold PBS, 25 μl of PI (50 μg/ml) was added and fluorescence intensity was assessed using a flow cytometer with untreated cells as the control (Zwain et al., 2021).

2.6.4.2. Qualitative uptake. HDF-a cells were cultured at a density of $1x10^5$ cells/well on sterile coverslips within a 12-well plate and incubated at 37°C. After 24 h the wells were washed twice with 0.1 M PBS (pH 7.4). Subsequently, the cells were treated with R-LFX-CO-NLCs for 4 h at 37°C. The cells were fixed using 4% paraformaldehyde and counter stained with DAPI. Images were captured using a Zeiss confocal microscope (GmbH, Germany).

2.6.5. Endocytosis pathway elucidation

HDF-a and NHEK cells were seeded at a density of $5x10^4$ cells/well in a 12 well plate and incubated for 24 h. Endocytosis inhibitors *viz.* 0.45 M sucrose, cytochalasin B (5 μg/ml) and nystatin (5 μg/ml) diluted in media were used to inhibit clathrin pathway, macropinocytosis and caveolae/lipid rafts pathway, respectively (Zwain et al., 2021; Martins et al., 2012). Cells were also incubated at 4 ℃ for the inhibition of energy-dependent endocytosis. Cells were treated with R-LFX-CO-NLCs for 4 h and analysis was carried out on flow cytometer using the method given in section 2.6.4.1.

2.6.6. In vitro scratch wound assay

HDF-a were seeded in a 6-well plate at a density of 6 x 10^4 cells/well until complete monolayer of confluent cells was observed. The monolayer was scratched vertically with a sterile P200 micropipette tip. To remove any adhering debris, the wells were washed twice with PBS. The cells were treated with LFX, LFX-CO-NLCs and CO-NLCs diluted in the media at two different concentrations of 1 and 10 μg/ml. Gap closure was measured by capturing images at 0 and 24 h using optical microscope. Untreated cells served as control. The evaluation of wound closure was performed using the MRI wound healing tool plugin in ImageJ software (Suarez-Arnedo et al., 2020).

2.7. Microbiology studies

2.7.1. Agar well diffusion assay

The method is elaborated in supplementary information S5.

2.7.2. Determination of Minimum inhibitory concentration (MIC) and Minimum bactericidal concentration (MBC)

The method is elaborated in supplementary information S5.

2.7.3. Establishment of biofilms on medical plastic and glass surfaces

P. aeruginosa biofilms were established on sterile flat-bottom 96-well polystyrene microplates (Nunc™ Edge™, non-treated, ThermoFisher Scientific, UK) or on autoclave-sterilized borosilicate glass coverslips (22x22mm, No. 1 Thickness, ThermoFisher Scientific, UK). The wells received 100 μl of growth media and 10 μl of inoculum diluted in PBS to contain approximately 1000 CFU per well. In experiments using glass coverslips, the latter were placed inclined in non-treated flat-bottom polystyrene 6-well plates (Tissue culture plate, 734-2323, VWR International, UK) in a bed of sterile 1.5% agar in sterile distilled water (sdH_2O). Subsequently, 4 ml of growth media containing approximately 5000 CFU of *P. aeruginosa* inoculum were added to the well. After culture preparation, both 96-well microplates and glass coverslip-containing 6-well plates were incubated statically at 37°C for 24 h in a humidity chamber to allow for biofilm formation. Then, the supernatant was removed, and the wells received fresh media containing different concentrations of LFX, LFX-CO-NLCs and CO-NLCs. The 96-well microplate wells received 100μl, while the glass containing 6-well plate wells received 4 ml. The resulting microplates and plates were incubated for 24 h.

2.7.4. Crystal violet (CV) mediated microscopic examination and viability assessment of the effect of LFX-CO-NLCs on P. aeruginosa biofilms

Post-treatment, the wells of the microplates were washed twice with 1x PBS. For microscopy observation, the wells were stained with 100 μl of 0.1% CV at room temperature for 10 min. CV was removed and wells were gently washed with sdH_2O to remove excess CV. Plates were allowed to air dry before imaging. Wells were imaged under the microscope at 40x magnification. Post-imaging, CV was extracted using 30% (v/v) acetic acid in sdH_2O, incubating the plate for 15 minutes at 20°C and the resulting solution was then measured spectrophotometrically (OD_{565}). For the assessment of cell viability, supernatants were removed from biofilm wells and placed into sterile microcentrifuge tubes. Phosphate bufer saline (PBS) was added to wells containing biofilms, and biofilm cells were removed *via* mechanical scraping and resuspension. Supernatant and removed biofilm cultures were serially diluted in PBS and plated onto Luria-Bertani agar (LBA) plates, which were subsequently incubated overnight. Bacterial colonies were enumerated.

2.7.5. Live/dead staining and microscopic examination of LFX-CO-NLCs treated P. aeruginosa biofilms

After treatment, coverslips were washed by submerging in sterile 1x PBS that was subsequently drained. Coverslips were stained for 15 minutes (20°C, dark conditions) with the Syto9 (3.5 μM, 483/503nm) and PI (20 μM, 535/615nm) solution mix (20℃ in the dark) and subsequently washed with sdH_2O. Coverslips were water-mounted on glass slides prior to observation *via* oil immersion microscopy.

2.7.6. Nanoparticle internalization assay

The internalization of fluorescently labelled NLCs was studied in *P. aeruginosa* culture suspensions as well as biofilms on glass coverslips. For in suspension studies, inoculum was diluted to a starting OD_{600} of 0.01 in LB supplemented with R-LFX-CO-NLCs and incubated at 37°C for 24 h at 200 rpm. Periodically for 5 h, 1 ml of culture was extracted from the vials, centrifuged (13,000 rpm, 1 min), washed twice (1x PBS), fixed (4% formaldehyde in PBS for 15 min), and washed twice with sdH_2O to

remove excess fixative. A volume of 10 µl from the resulting suspensions was deposited on a 0.01% Poly-L–Lysine (PLL) coated glass slide. Following water mounting and nail varnish sealing, the samples were visualised immediately or stored at 4°C until use. For biofilm studies, biofilms established on glass coverslips were treated with R-LFX-CO-NLCs containing Luria-Bertani (LB) medium as above for 24 h at 37°C statically.

2.7.7. Image capture and analysis

CV-stained biofilm samples were observed at 40x magnification using light microscopy with a Nikon Eclipse E200 (E Plan 4x/0.10 WD30). Live/dead and R-LFX-CO-NLCs stained cell suspension and biofilm samples were observed using oil immersion DIC and fluorescence microscopy (Zeiss Axio Observer, 630x Apochromat 63x/1,4 Oil DIC). Image capture was undertaken using the inbuilt Axiocam. Biomass quantitation determinations from CV-stained samples were undertaken using ImageJ (Fiji platform). Excitation and emission of fluorophores are as follows: Rhodamine123, 508/528 nm, Syto9, 483/503 nm, PI, 535/615 nm.

2.8. In vivo murine burn wound infection study

2.8.1. Animal ethical compliance

Animal studies were approved by Institutional Animal Ethics Committee (PU/45/99/CPCSEA/IAEC/2019/290) and the Institutional Biosafety Committee (IBSC/PU/2019/135) at Panjab University. Male BALB/c mice were acquired from the Central Animal House of Panjab University, India. The animals, aged between 4 to 8 weeks and weighing (20–25 g), were housed in well-ventilated rooms that maintained a 12 h light/dark cycle and a stable temperature of 25 ± 2°C within clean plastic cages. They were provided with a standard rat diet (Hindustan Lever, Mumbai), and fresh water was continuously available.

2.8.2. Efficacy study in Pseudomonas aeruginosa PAO1 biofilm infected burn wound in mice

A murine burn wound infection model was established, as previously reported (Gupta et al., 2015). A burn wound was induced by applying a heated brass rod (10x10 x100 mm) to the dorsal area of mice that had been anesthetized through an intraperitoneal injection (I/P) of xylazine (10 mg/ml) and ketamine (80 mg/kg). To infect the burn site, 50 µl of *P. aeruginosa* inoculum (10^4 CFU/ml) was applied topically and 48 h were allowed for biofilm formation before any treatment was started. The health of the mice was monitored throughout the period of study.

The mice were divided into four groups (n=9/group). Group 1 did not receive any treatment (control group). Groups 2, 3, 4 received treatments with LFX-CO-NLCs hydrogel, CO-NLCs hydrogel and plain LFX gel respectively. The gels were applied at the infection site twice a day over a duration of 15 days. The progression in wound closure was assessed by using ImageJ software to analyze the digital photos of wounds taken on days 0, 1, 3, 7, 10, and 15 and measuring the percentage change from the initial wound size. On days 1, 7, and 15 following the treatment, three mice from each group were anesthetized to collect the wound tissue followed by sacrificing by cervical dislocation. The efficacy of the therapy was assessed using various measures. The impact of the treatment on the wound biofilm was investigated by analyzing the tissue samples (collected on day 1 after the treatment) fixed in 10% buffered formalin on FESEM (Hitachi SU8010, Japan). The bacterial load (CFU/ml) was determined by plating homogenized tissue samples extracted on days 1, 7, and 15 post-treatments on nutrient agar plates. Histopathological analysis was carried out using haematoxylin and eosin (H&E), and Masson's trichome (MT) staining of fixed tissue samples obtained on days 1 and 15 post-treatment. The sections were captured utilizing the Olympus DP80 imaging system (Olympus, Japan). The antioxidant activity in infected wound tissue homogenates was evaluated by lipid peroxidation through malondialdehyde levels and glutathione, superoxide dismutase, and catalase activity, following methodologies outlined in prior research (Saha et al., 2023).

2.9. Statistical analysis

The data are presented as mean ± standard deviation. To assess the statistical significance of the findings from the murine burn wound model, a two-way ANOVA was conducted, followed by a post hoc Bonferroni test. Results were deemed statistically significant at levels of (*) $p < 0.05$ and (**) $p < 0.001$. Statistical analyses were performed using GraphPad Prism 7.0. The bacterial counts were reported as Log10 values.

3. Results

3.1. Solubility study

LFX showed highest solubility of 100.12 ± 1.24 mg/g in stearic acid followed by Precirol ATO5 (30.01 ± 1.15 mg/g) hence these two lipids were selected for preparation of NLCs. Solubility in Compritol 888 ATO and Dynasan 114 was found to be low (15.50 ± 1.55 mg/g).

3.2. Preparation of LFX loaded nanostructured lipid carriers and optimization

NLCs prepared using stearic acid (particle size 215.40 ± 3.33nm and PDI 0.254 ± 0.008) showed a creamy consistency and became highly viscous after 4–6 h of preparation (Müller et al., 2002) hence were not carried forward and Precirol was used as solid lipid for NLCs preparation, and their evaluation parameters are presented in Table 1. Stable NLCs (PS 185.5 ± 4.1, PDI 0.286 ± 0.012) were formed with 2.5% Span 80. EE was found to be low (31.23 ± 0.54%) at LFX concentration of 1% which was improved by reducing the LFX to 0.75% (37.44 ± 0.69%) and 0.5% (42.11 ± 0.64%), respectively. The increase in EE observed at lower drug loading can be attributed to the avoidance of lipid matrix saturation, allowing more efficient incorporation of the drug within the NLC system. At reduced concentrations, the drug is better accommodated within the lipid matrix, minimizing expulsion and partitioning into the external phase, which ultimately enhances entrapment efficiency (Müller et al., 2002; Das et al., 2012).

Higher lipid concentration in the NLCs significantly increased EE to 60.15 ± 0.28% probably due to its ability to entrap more LFX which could be further increased to 63.72 ± 0.94%, when LFX concentration was reduced to 0.25%. This agrees with the previous report where decreasing the amount of drug added and/or increasing the lipid content led to an increment in EE of LFX (Beraldo-Araújo et al., 2022). Increasing Span 80 led to reduction in EE which could be due to higher drug solubilizing capacity of the surfactant leading to more drug remaining in the aqueous phase. Increase in co-surfactant concentration (1.5%) led to thickening of NLCs. Therefore, formulation B5 with LFX at 0.5% concentration (Table 1) was selected as optimized NLCs and was referred to as LFX-CO-NLCs. LFX at 0.5% concentration is used in a commercially available ophthalmic solution though no topical product of LFX is available commercially and this is also in agreement with a previous report (Koch et al., 2005).

3.3. Physicochemical characterization of NLCs

3.3.1. Particle distribution, Zeta potential and Transmission electron microscopy

TEM analysis revealed LFX-CO-NLCs to be spherical in shape and no aggregation of nanoparticles (Fig. 1B) Hydrodynamic diameter as determined by dynamic light scattering was found to be 169.9 nm with PDI of 0.227 and ZP as −43.1 mV (Fig. 1C,D).

3.3.2. Differential scanning calorimetry

Pure LFX exhibited four endothermic peaks. The first broad

Table 1
Composition and characterization of integrated biofunctional nanostructured lipid carriers.

Formulation code	Precirol (% w/w)	Clove oil (%w/w)	Span 80 (%w/w)	Sodium cholate (%w/w)	LFX (% w/w)	Particle size (nm)	PDI	Zeta potential (mV)	TDC (%)	EE (%)
B1	3	3	2	1	1	–	–	–	–	–
B2	3	3	2.5	1	1	185.5 ± 4.1	0.286 ± 0.012	−45. 20 ± 2.41	99.01 ± 0.82	31.23 ± 0.54
B3	3	3	2.5	1	0.75	163.3 ± 3.2	0.221 ± 0.016	−44.70 ± 2.17	99.86 ± 0.51	37.44 ± 0.69
B4	3	3	2.5	1	0.5	152.0 ± 1.7	0.222 ± 0.015	−42.50 ± 1.91	100.02 ± 0.48	42.11 ± 0.64
B5	4	4	2.5	1	0.5	169.9 ± 3.1	0.227 ± 0.010	−43.1 ± 2.22	98.86 ± 0.74	60.15 ± 0.28
B6	4	4	2.5	1	0.25	162.8 ± 3.3	0.231 ± 0.016	−44.90 ± 0.55	98.15 ± 1.15	63.72 ± 0.94
B7	4	4	3.5	1	0.5	172.1 ± 3.0	0.226 ± 0.011	−48.30 ± 2.96	99.97 ± 0.56	52.66 ± 0.63
B8	4	4	4.5	1	0.5	180.9 ± 3.6	0.233 ± 0.013	−45.30 ± 2.26	100.09 ± 0.17	49.26 ± 1.18
B9	5	5	2.5	1	0.5	201.4 ± 1.8	0.274 ± 0.006	−42.36 ± 1.86	100.16 ± 0.59	55.56 ± 0.98
B10	4	4	2.5	1.5	0.5	–	–	–	–	–

endothermic peak was detected between 50 and 110°C, indicating dehydration during heating. The literature reports of LFX thermal analysis showed this peak in the range of 50–90°C. However, use of hermetically sealed pan led to increased pressure which resulted in dehydration taking place at higher temperature. The remaining three peaks denoting the melting of the γ, β and α forms of LFX were observed at 227.36°C, 231.35°C and 235.35°C respectively (Fig. 2A) that correlated closely with those documented in the existing literature (Gorman et al., 2012). Precirol exhibited melting endotherm at 67.25°C (Dolatabadi et al., 2021). Physical mixture of Precirol and CO showed endothermic peak at 53.13°C which was at lower temperature than for pure Precirol. CO led to depression in melting point of Precirol demonstrating disordered state of the crystals and creation of lattice defects whereas the endothermic peak for CO-NLCs was observed at 59.26°C. LFX-CO-NLCs presented only one melting endothermic peak at 60.32°C but no event due to LFX melting was observed, which suggests that LFX may have dissolved and integrated into the lipid mixture and transformed into an amorphous state after encapsulation into the NLCs.

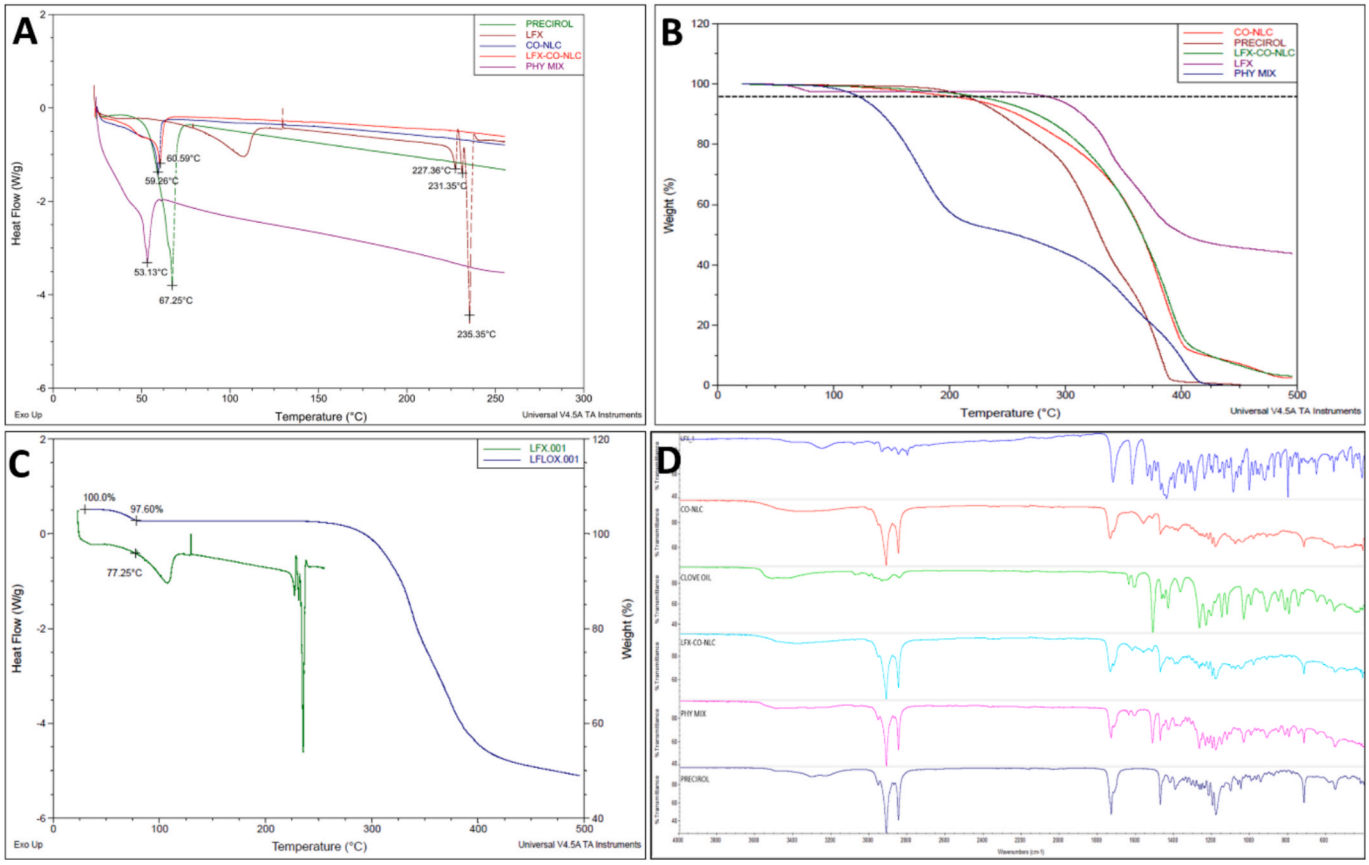

Fig. 2. Overlay of **(A)** DSC thermographs, **(B)** TGA thermographs of LFX, LFX-CO-NLCs and excipients. **(C)** DSC and TGA thermographs of LFX and **(D)** FTIR spectra of LFX, LFX-CO-NLCs and excipients. Abbreviations- LFX: levofloxacin, DSC: Differential scanning calorimetry, TGA: Thermogravimetric analysis, FTIR: Fourier transform infrared.

3.3.3. Thermogravimetric analysis (TGA)

The thermal decomposition of the samples upon heating is illustrated through TGA. The theoretical water content (2.43%) of LFX hemihydrate is in agreement with weight loss of 2.40% (w/w) measured on the LFX thermogram, which corresponds to an endothermic event observed at ~78 °C (Fig. 2C) (Gorman et al., 2012). LFX showed major degradation at around 290°C (5% weight loss). Precirol is a stable lipid and showed about 5% weight loss at 219°C. However, physical mixture of clove oil and Precirol showed 5% weight loss at about 125°C with almost 50% decomposition at ~255°C in comparison to 50% weight loss of Precirol at ~329°C. CO-NLCs showed 5% weight loss at 215°C whereas LFX-CO-NLCs showed the same at ~233°C which is similar to degradation of solid lipid Precirol. This shows that LFX was well integrated into the lipid matrix (Fig. 2B).

3.3.4. Fourier-transform infrared spectroscopy

The LFX spectrum exhibited several distinctive peaks, including: 3265.23 cm^{-1}, indicative of carboxylic acid (O–H stretching); 2932.14 cm^{-1}, associated with CH_3 (C–H stretching); 3081 cm^{-1}, characteristic of aromatic compounds (C–H stretching); 799.82 cm^{-1}, representing aromatic C–H bending; 1723 cm^{-1}, corresponding to C=O stretching; 1618.94 cm^{-1}, related to aromatic C=C stretching; 1294.37 cm^{-1}, linked to amine C–N stretching; and 1086.18 cm^{-1}, denoting C–F stretching (Fig. 2D) (Razdan et al., 2022). Precirol exhibited strong bands at 1792 cm^{-1} (Carboxylic acid; C=O stretching), 2912.85 and 2848.34 cm^{-1} (free CH_3; C–H stretching), 1471.05 cm^{-1} ($–CH_2–CH_2$; C–H bending), 1195.99 and 1178.08 cm^{-1} (alcoholic OH group; C–O stretching), 3200–3300 cm^{-1} (carboxylic acid; O–H stretching). Pure CO spectrum showed high numbers of peaks indicating the presence of various volatile compounds with peaks at 3510 cm^{-1} (phenol; O–H stretching), 1605 and 1511 cm^{-1} (aromatic; C=C stretching), 1231 and 1032 cm^{-1} (arylether; C–O–C stretching) and 849 and 793 cm^{-1} due to C–H bending of aromatic ring. LFX-CO-NLCs showed characteristic peaks seen for Precirol at 2913.05 and 2848.58 cm^{-1} which were observed in CO-NLCs as well. There were slight shifts observed in the peaks of LFX. The broad O–H stretch could be due to overlapping functional groups of other excipients and LFX. The characteristic peaks of LFX corresponding to O–H stretch of carboxylic acid group at 3379.56 cm^{-1}, aromatic C=C stretching at 1618.73 cm^{-1}, C–N stretching at 1265.74 cm^{-1} and C–F stretching at 1076.53 cm^{-1} were observed in LFX-CO-NLCs. However, the decrease in characteristic peak intensity can be attributed to the successful encapsulation of the drug within the lipid matrix, where the drug molecules are molecularly dispersed or solubilized, leading to reduced exposure of functional groups to infrared radiation. Additionally, the presence of lipid and surfactant components may mask or overlap with the drug's characteristic peaks, resulting in diminished signal intensity. Importantly, the absence of significant peak shifts or the appearance of new peaks indicates that no chemical interaction or degradation has occurred, confirming the physicochemical compatibility of the drug with the NLC components (Teng et al., 2019).

3.4. Gas-chromatography mass spectrometry (GC-MS) analysis

GCMS spectrum of CO identified compounds present in the sample along with their percentage compositions (Table S1). Eugenol emerged as the predominant component of the clove oil, constituting 53.10%, which aligns well with findings from prior studies (Hemalatha et al., 2016). Other major components were β-caryophyllene (14.79%), α-humulene (8.05%) and campesterol (8.76%). The LFX-CO-NLCs chromatogram (Fig. S1) illustrates the peaks of eugenol (RT:7.16 min), β-caryophyllene (RT:8.06 min) and α-humulene (RT:8.50 min) with few peaks of minor components confirming that CO was successfully integrated in the solid lipid matrix of NLCs without any functional changes.

3.5. Preparation and characterization of LFX-CO-NLCs hydrogel

The pH of the LFX-CO-NLCs hydrogel was found to be 5.81 ± 0.18, making it acceptable for topical administration and lowering wound pH which may help to slow the infectious bacterial growth. LFX-CO-NLCs hydrogel exhibited drug content of 99.29 ± 1.09% which demonstrated that there is no drug-Carbopol hydrogel interaction. Rheological characterization of LFX-CO-NLCs hydrogel (Fig. 3B) reveals its ability to spread over skin. The viscosity of the hydrogel was seen to decrease as the shear rate was increased. The viscosity decreased from 37,400 mPa-s to 2370 mPa-s upon raising the shear rate from 5 to 120 s^{-1}. This demonstrates the LFX-CO-NLCs hydrogel's pseudoplastic (shear-thinning) capabilities, which will facilitate topical application. The textural profile of LFX-CO-NLCs hydrogel showed that it had respectable strength, spreadability, and extrusion properties (Fig. 3A). The values determined for firmness, consistency, cohesiveness, and work of cohesion were 4312.7 g, 6507.46 g.s, –2197.73 g and −2227.3 g.s, respectively.

3.6. In vitro drug release

Fig. 3C shows the drug release profiles of LFX-CO-NLCs, LFX-CO-NLCs hydrogel and plain LFX gel. Two distinct phases of drug release were observed: an early burst phase and a steadier sustained release phase. LFX-CO-NLCs showed an initial burst release of 60.23 ± 1.56%, whereas LFX-CO-NLCs hydrogel had a burst release of 31.18 ± 1.26% after 15 min. Incorporation of LFX-CO-NLCs in the hydrogel base reduced the initial burst release and provided the release in a sustained manner. Plain LFX gel showed initial burst release of 29.69 ± 1.57% in 15 min but released up to 75.57 ± 2.87% of the drug after 8 h, whereas LFX-CO-NLCs hydrogel showed complete drug release of 99.01 ± 1.87% at the same time. The Carbopol hydrogel network acts as an additional diffusion barrier, restricting drug mobility and thereby retarding the release rate. The incorporation of NLCs into Carbopol hydrogel provides a synergistic system that enhances controlled drug delivery governed by a dual-controlled mechanism through combined lipid–polymer diffusion barriers (Pople and Singh, 2006).

3.7. Stability studies

Stability studies of LFX-CO-NLCs showed no significant change in PS of LFX-CO-NLCs over a period of 6 months when stored at 25°C. However, PS increased significantly at storage of 40°C from 164.3 ± 2.8 to 196.1 ± 3.2 nm ($P<0.05$). This could be attributed to increased kinetic energy of the system at higher temperature (40 °C/75% RH) leading to enhanced particle collision and subsequent particle aggregation. Even though this change was significant, the PS remained below 200 nm and within the acceptable limit. No cracking and sedimentation were observed during the study period, PDI of the formulation remained stable throughout the period of 6 months at all conditions (Table S2). No significant change in pH, appearance and% drug content of LFX-CO-NLCs hydrogel was observed following 6 months of stability study (Table S3).

3.8. Cell line studies

3.8.1. Cell viability study

Cell proliferation studies showed no toxicity with any of the treatments at all tested concentrations after 24 h with cell viability >70% in both the cells. However, after 48 h LFX showed cellular toxicity at higher concentrations of 20 and 50 μg/ml showing cell viability of 68.48 ± 1.80% and 52.16 ± 1.46% in HDF-a cells and 63.26 ± 2.12% and 44.68 ± 1.98% in NHEK cells respectively. Treatment with LFX-CO-NLCs and CO-NLCs did not show any toxicity after 48 h which reveals biocompatibility for topical application (Fig. 4A).

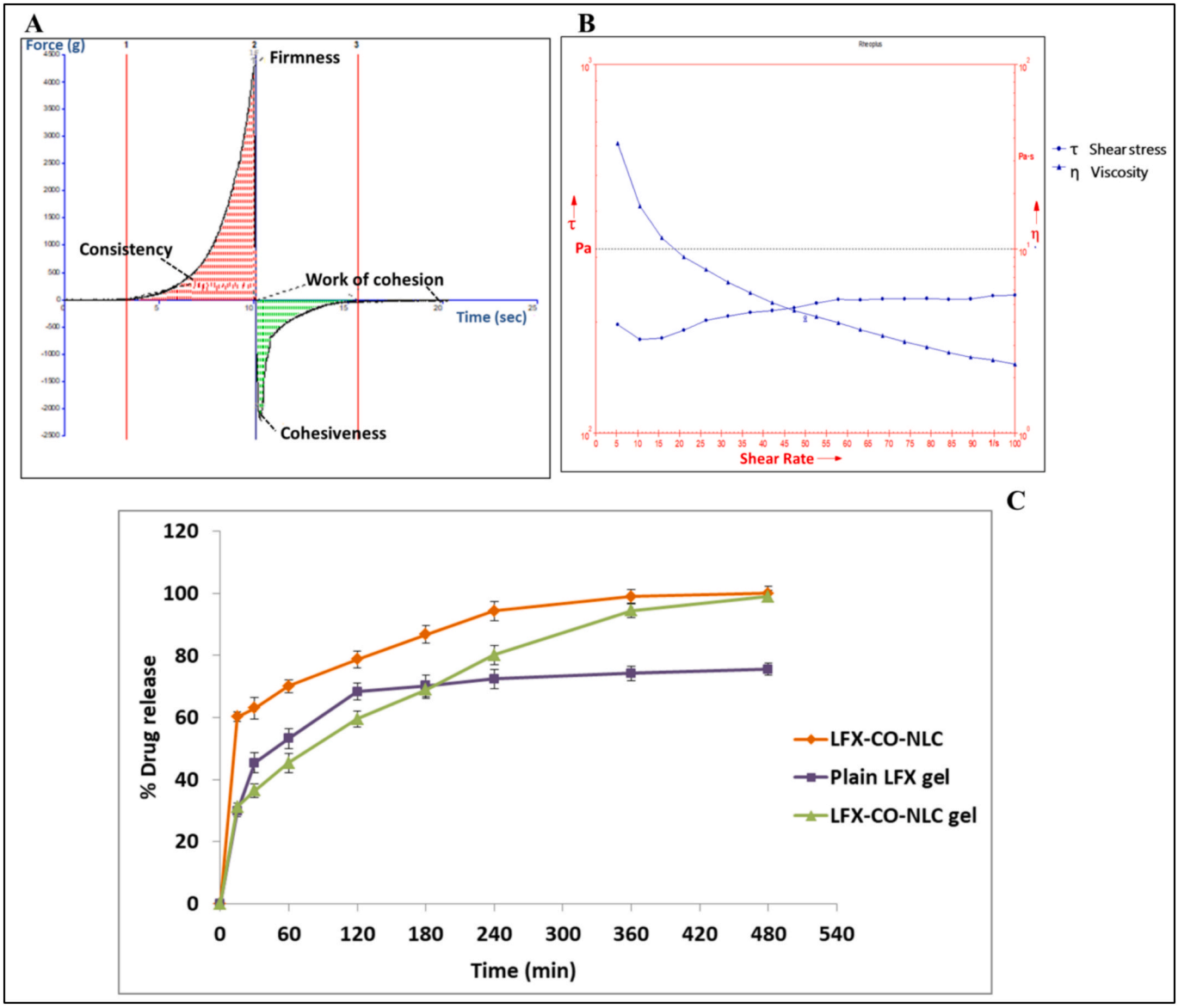

Fig. 3. Graphs of **(A)** texture profile and **(B)** rheology of LFX-CO-NLCs hydrogel and **(C)** Drug release profile curve of LFX-CO-NLCs hydrogel in comparison to LFX-CO-NLCs and pure LFX in gel.

3.8.2. *Cell cycle analysis*

It was observed that in control group, 67.85 ± 0.52%, 8.61 ± 0.33% and 22.5 ± 0.39% of HDF-a cells were in G0/G1, S and G2/M phases, respectively (Fig. 4B). Treatment with LFX at concentrations of 1 and 10μg/ml led to slight increase in G0/G1 population to 72.71 ± 2.20% and 71.29 ± 1.98%, respectively in comparison to control whereas minor reduction in S and G2/M phase populations was seen. However, treatment with LFX-CO-NLCs at concentrations of 1μg/ml led to slight increase in S and G2/M phase populations to 10.23 ± 0.99% and 25.02 ± 1.50%, respectively whereas treatment at 10 μg/ml led to increment in S and G2/M phase populations to 11.69 ± 0.82% and 25.15 ± 1.36%, respectively. CO-NLCs showed ~2-fold increase in S phase population in comparison to control (Fig. 4B). Overall, this study demonstrates that treatment with NLCs did not lead to cell cycle blockage and rather promoted the progression of cell cycle.

3.8.3. *Cellular uptake studies*

Quantitative uptake study revealed concentration-dependent uptake of R-LFX-CO-NLCs in both HDF-a and NHEK cells as depicted by shifts in flow cytometer histograms (Fig. 5 A-C). Fluorescence microscopy images revealed uptake of R-LFX-CO-NLCs in HDF-a cell lines with NLCs distributed in the cytoplasm and no uptake in the nucleus (Fig. 5G).

3.8.4. *Mechanism of cellular uptake*

When HDF-a and NHEK cells were incubated with R-LFX-CO-NLCs at 4°C for 4h, the uptake was considerably lower in terms of mean fluorescence intensity in comparison to incubation at 37°C (Fig. 5 D-F) demonstrating that NLCs uptake into cells is an energy-dependent process. Endocytosis of NLCs into the cells, may result from the interaction of many pathways. Macropinocytosis (cytochalasin B inhibition) emerged as the dominant internalisation pathway for R-LFX-CO-NLCs as uptake was reduced by 6.3-folds and 4.6-folds for HDF-a and NHEK cells, respectively in comparison to control ($P<0.001$). However, clathrin-mediated uptake (inhibited by sucrose) can also be strongly attributed for uptake of R-LFX-CO-NLCs into the cells as it was reduced by 5.3-folds and 3.4-folds for HDF-a and NHEK cells, respectively in comparison to control ($P<0.001$). Caveole/lipid rafts pathway (inhibition by nystatin) also contributed for uptake of R-LFX-CO-NLCs as evident by 1.5- and 1.7-folds reduction of uptake in comparison to control ($P<0.001$) for HDF-a and NHEK cells, respectively This is in agreement with earlier

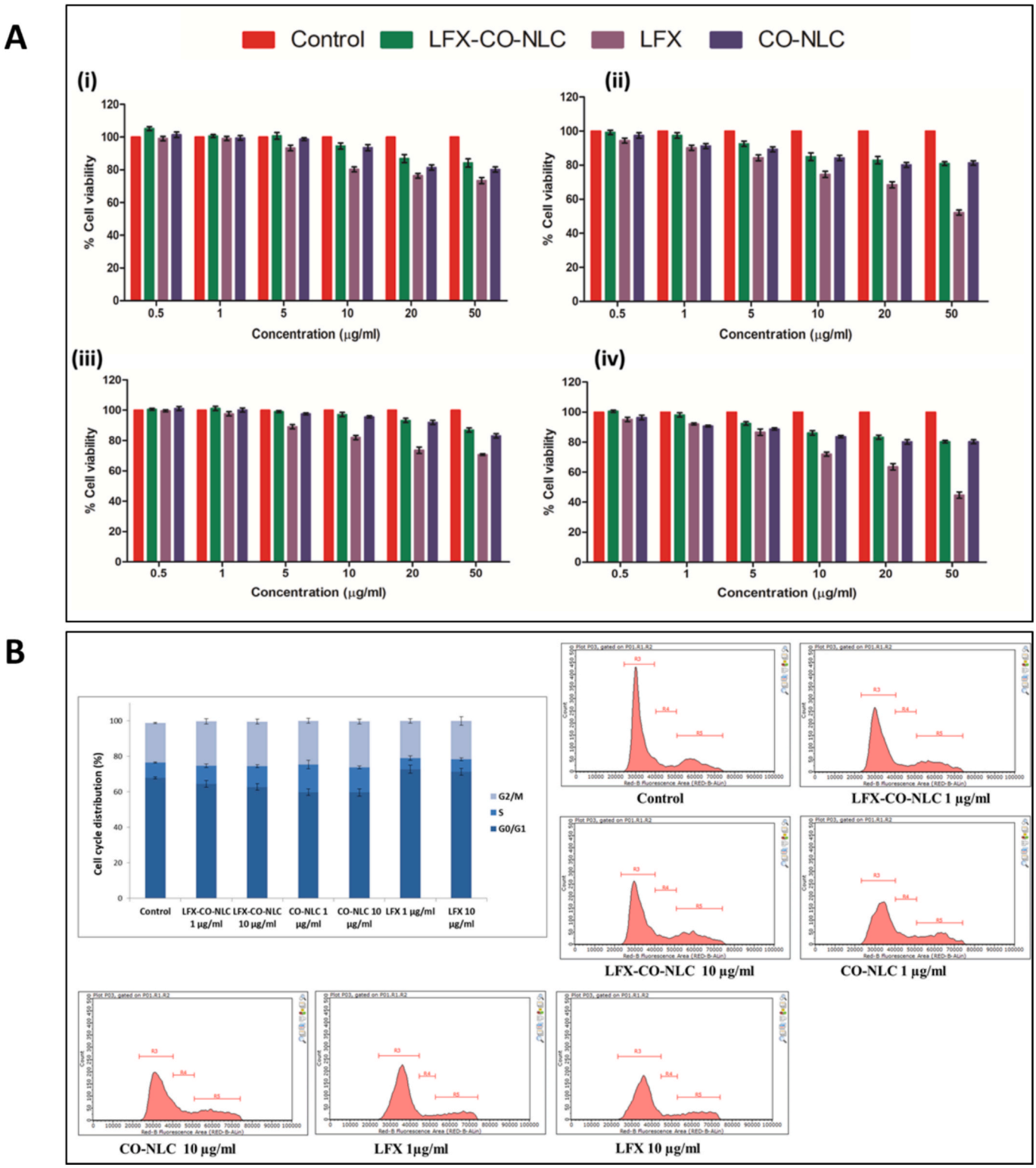

Fig. 4. **(A)** Cell viability study of LFX-CO-NLCs in HDF-a cells for **(i)** 24 h and **(ii)** 48 h and NHEK cells for **(iii)** 24 h and **(iv)** 48 h using Presto Blue assay. **(B)** Cell cycle distribution histogram for control, LFX-CO-NLCs, LFX and CO-NLCs treated HDF-a cells following 24 h of incubation. Also, shown are flow cytometer histograms of cell cycle distribution. Data is expressed as mean ± SD (n = 3). Abbreviations- LFX: levofloxacin, LFX-CO-NLCs: levofloxacin and clove oil loaded nanostructured lipid carriers, CO-NLCs: clove oil NLCs, HDF-a: human dermal fibroblasts-adult, NHEK: normal human epidermal keratinocytes.

studies which demonstrated that more than one routes can be used to internalise lipid nanoparticles (Silva et al., 2017; Zwain et al., 2023).

3.8.5. *In vitro scratch wound assay*

Scratch test is a frequently used *in-vitro* method for determining wound healing activity of various compounds (Liang et al., 2007). Untreated control showed only 35.12 ± 2.50% wound closure after 24 h whereas LFX-CO-NLCs demonstrated wound closure of 64.78 ± 4.15% and 90.55 ± 4.75% in comparison to control ($P < 0.001$) at concentrations of 1 and 10 µg/ml, respectively. CO-NLCs and LFX at 10 µg/ml

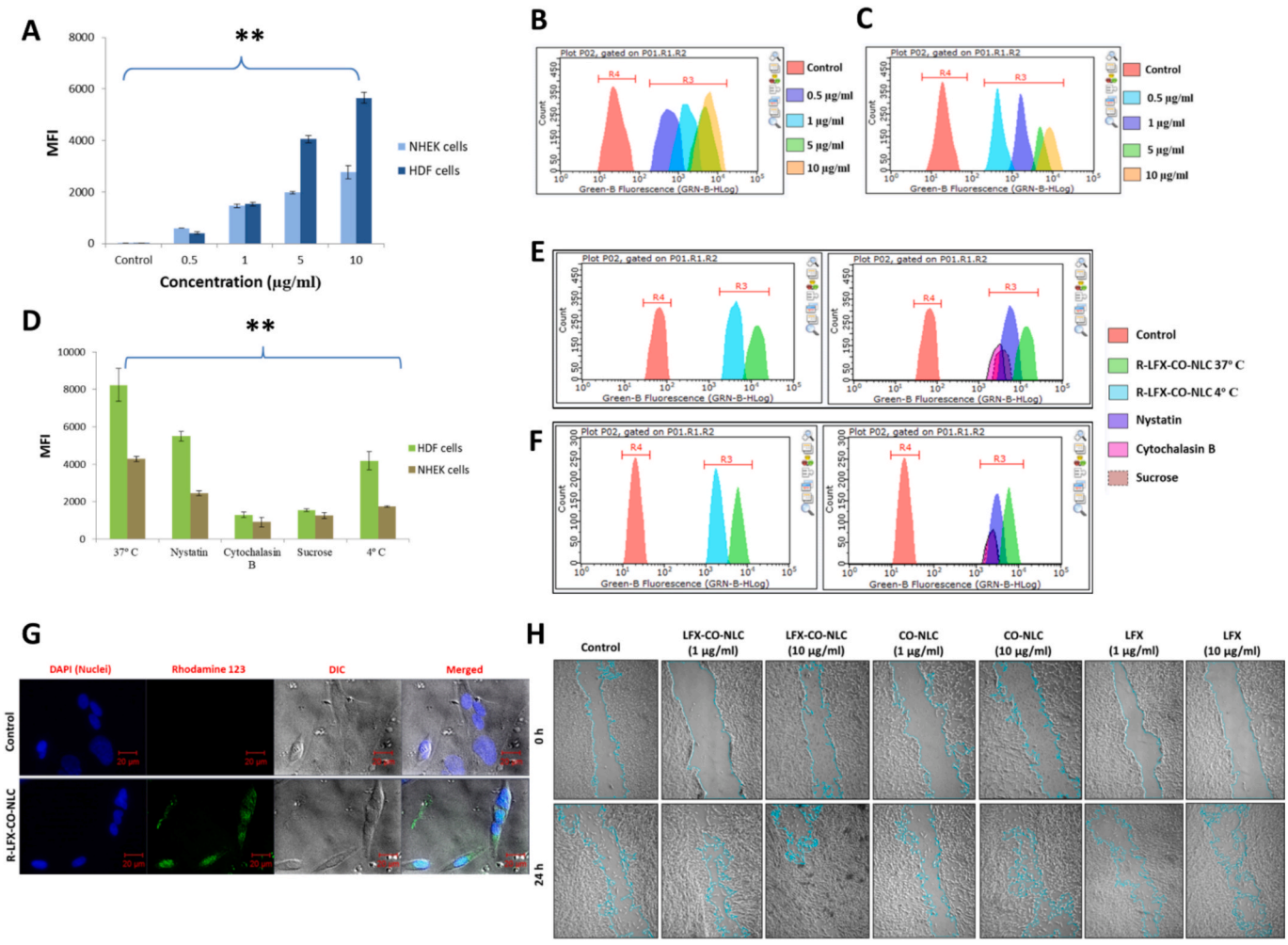

Fig. 5. **(A)** Bar graph of MFI vs concentration. Flow cytometer histogram showing concentration-dependent uptake of R-LFX-CO-NLCs in **(B)** HDF-a **and (C)** NHEK cells. **(D)** Determination of endocytosis pathways following treatment of HDF and NHEK cell lines with various inhibitors, graph showing MFI bar chart. Flow cytometer histograms before and after incubation of R-LFX-CO-NLCs in the presence of inhibitors in **(E)** HDF-a and **(F)** NHEK cells. **(G)** Fluorescence microscopy images showing cellular uptake of R-LFX-CO-NLCs in HDF-a cells shown by green fluorescence, blue fluorescence refers to DAPI stained nuclei. **(H)** Images of *in vitro* scratch wound assay in HDF-a cells. Untreated control is represented by R4 and R3 represents a region for the shifted peaks. $^{**}P < 0.001$ in comparison to untreated control. Abbreviations- R-LFX-CO-NLCs: Rhodamine 123 labelled LFX-CO-NLCs, HDF-a: human dermal fibroblasts-adult, NHEK: normal human epidermal keratinocytes. MFI- mean fluorescence intensity.

concentration showed wound closure of 65.47 ± 3.87 and 60.15 ± 4.13%, respectively as compared to control (P <0.05) demonstrating wound healing potential of LFX-CO-NLCs (Fig. 5H).

3.9. Microbiology studies

3.9.1. Agar well diffusion assay

LFX-CO-NLCs showed higher zone of inhibition (ZOI) for all tested pathogens in comparison to LFX solution (P<0.01) (Table 2). CO-NLCs showed smaller ZOI but incorporation of CO and LFX in NLCs demonstrated synergistic effect as evidenced by higher ZOI of LFX-CO-NLCs.

Table 2
Zone of inhibition diameters determined using agar well diffusion assay.

Bacteria	Zone of inhibition (mm)		
	LFX	LFX-CO-NLCs	CO-NLCs
***E. coli* MTCC 1687**	42.5 ± 1.2	45 ± 0.5 *	9 ± 1.2
***P. aeruginosa* PAO1**	43.2 ± 0.9	49.3 ± 1.1 *	9.5 ± 0.5
***S. aureus* P-13138**	23.5 ± 0.7	32.3 ± 0.4 *	8.2 ± 0.8
***S. aureus* (MRSA) MTCC 43300**	40.5 ± 0.5	42.7 ± 0.3 *	6.5 ± 0.5

*$P < 0.05$ in comparison to pure levofloxacin solution and CO-NLCs.

3.9.2. Determination of minimum inhibitory concentration (MIC) and minimum bactericidal concentration (MBC)

The MIC values for LFX-CO-NLCs were found to be significantly lower in all tested strains in comparison to free LFX solution (Table 3).

Table 3
MIC and MBC of LFX, LFX-CO-NLCs and CO-NLCs against a range of pathogens.

Strain	MIC of LFX (µg/ml)	MIC of CO-NLCs (µg/ml)	MIC of LFX-CO-NLCs (µg/ml)	MBC of LFX (µg/ml)	MBC of CO-NLCs (µg/ml)	MBC of LFX-CO-NLCs (µg/ml)
***E. coli* MTCC 1687**	2	128	0.5*	4	256	1*
***P. aeruginosa* PAO1**	2	128	0.5*	4	256	1*
***S. aureus* P-13138**	2	64	1*	4	128	2*
***S. aureus* (MRSA) MTCC 43300**	4	64	2*	8	128	4*

*$P < 0.05$ in comparison to pure levofloxacin solution.

There was 4-fold reduction in MIC against *E. coli and P. aeruginosa*, and 2-fold reduction against *S. aureus* in comparison to LFX solution ($P<0.001$). Similar reduction was observed in MBC values. CO-NLCs relatively showed weak antibacterial activity with high MIC values for all tested strains.

3.9.3. Antibiofilm studies

3.9.3.1. Effect of LFX-CO-NLCs on the P. aeruginosa biofilm mass. The observation of microscopy images of 24 h-formed *P. aeruginosa* biofilms stained with CV revealed a distinctive decrease on surface coverage when they were treated with LFX solution. The decrease was enhanced when the antibiotic was delivered as LFX-CO-NLCs (Fig. 6A i-iv). The enhanced antibiofilm effect was observed at both the MIC (0.5 μg/ml)

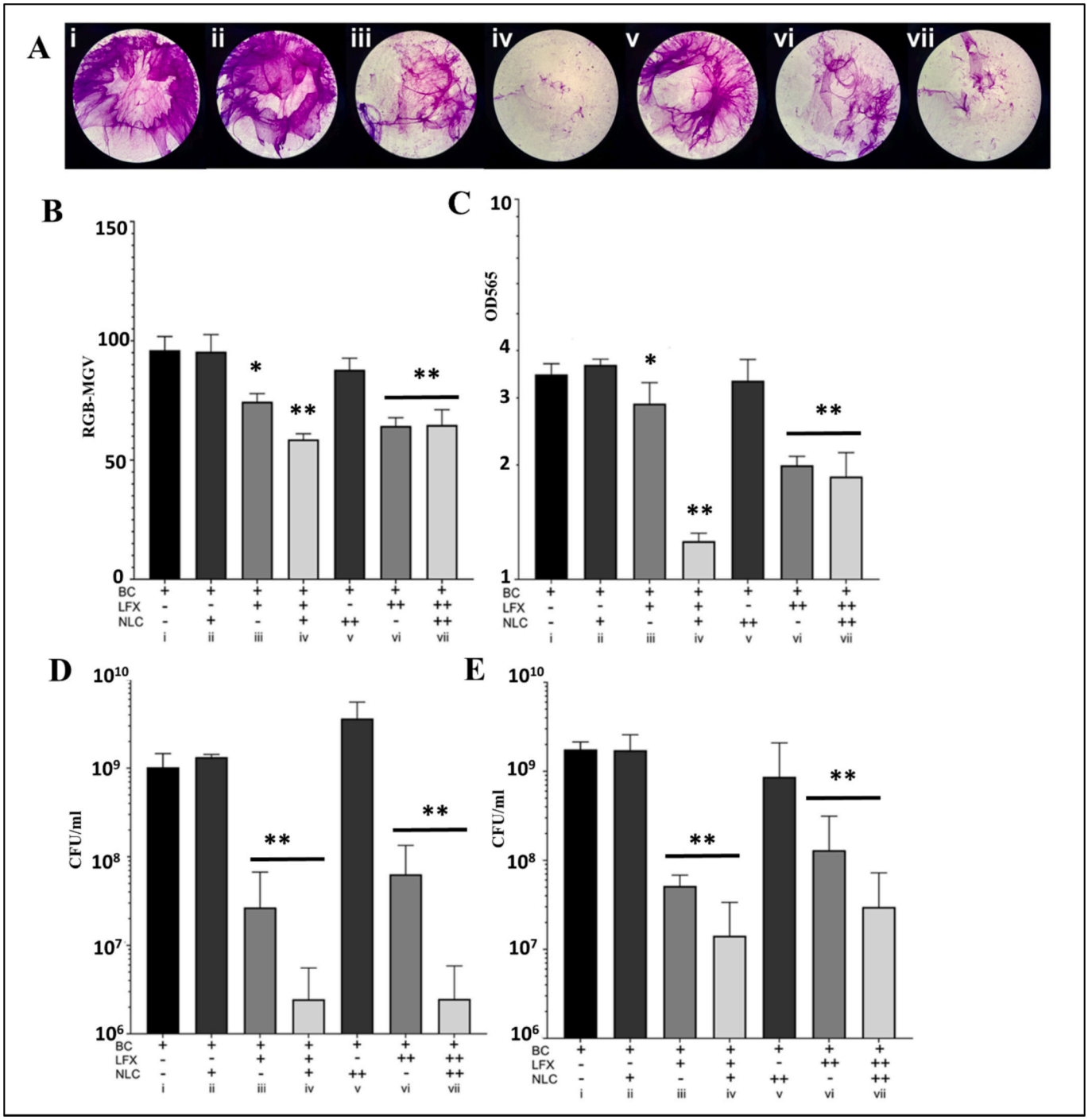

Fig. 6. Biomass determinations from a surface colonisation experiment of *P. aeruginosa* PA01, indicated by; **(A)** light microscopy images of crystal violet-stained biofilms (40x) (i:untreated bacterial biofilm, ii: biofilm treated with CO-NLCs at 0.5 μg/ml, iii: LFX treated biofilm at 0.5 μg/ml, iv: LFX-CO-NLCs treated biofilm at 0.5 μg/ml, v: biofilm treated with CO-NLCs at 1.0 μg/ml, vi: LFX treated biofilm at 1.0 μg/ml vii: LFX-CO-NLCs treated biofilm at 1.0 μg/ml). (**B**) quantification of the inverse mean grey value (MGV) of 16-bit converted images using the software ImageJ, indicating biomass remaining, and (**C**) crystal violet dissolution in acetic acid (30%) and spectrophotometric measurement at 565nm. Bacterial viability by colony counting in LFX, CO-NLCs & LFX-CO-NLCs treated **(D)** planktonic and **(E)** biofilm phase *P. aeruginosa* in a surface colonisation experiment. $^{**}P < 0.001$ and $^{*}P < 0.05$ in comparison to untreated bacterial control.

and MBC (1μg/ml) of LFX-CO-NLCs. However, the reduction in biofilm mass was more pronounced at MIC. The results from the microscopy image observation were consistent with image analysis determinations of CV-stained biofilm and with spectrophotometric analysis of the chemically extracted dye. Biofilm treated with pure LFX at 0.5μg/ml had a biofilm biomass similar to the untreated control (Fig. 6B i). In contrast, the impact on biomass density of LFX-CO-NLCs is particularly noticeable and statistically significant at those lower concentrations when compared to the LFX sample biofilm (Fig. 6 B/C iv). The finding highlights the fact that LFX-CO-NLCs at concentration of 0.5 μg/ml has a higher antibacterial and antibiofilm activity than the equivalent LFX concentration. In turn, the observation of lesser antibiofilm activity by the LFX-CO-NLCs (in comparison to LFX) at higher concentration of 1 μg/ml can be due to the fact that the high antibiotic concentration in the LFX sample is sufficient to lead a significant drop on biofilm biomass, thus minimizing the difference of the enhanced effect introduced by the LFX-CO-NLCs.

3.9.3.2. Effect of LFX-CO-NLCs on the viability of P. aeruginosa biofilm. To get an understanding of cell viability, both on the supernatant covering the biofilm and the biofilm itself, samples were taken from both the sites. The supernatant was directly plated on culture medium plates while biofilms were mechanically removed and resuspended in PBS prior to plating. Consistent with the results obtained from differential biomass determinations above, viability enumerations of liquid cultures with non-loaded antibiotic NLCs did not affect the viability of either planktonic or biofilm cultures compared to the non-supplemented control. Similarly, LFX alone was bactericidal to both culture types with a similar killing at both antibiotic concentrations. Importantly, LFX-CO-NLCs at both the concentrations (0.5 and 1 μg/ml) distinctively improved the antimicrobial effect as compared to the antibiotic in suspension alone (Fig. 6D iv & vii). The physiological tolerance of the biofilm to antimicrobials has been previously assigned to their slower growing phenotype and other characteristics of biofilms (Vestby et al., 2020). It is also to be noted that the bacteria in the supernatant samples must have derived from the biofilm that had formed, as bacterial cells in suspension growing from the original inoculum were removed after biofilm formation, before treatment administration. Consequently, it is possible that the antibiotic tolerance of those dispersal-derived bacteria in suspension may overestimate the resistance of planktonic cells in exponential cultures. Our results suggest that biomass is not a direct reflection of viability at least in our strain under the conditions used for

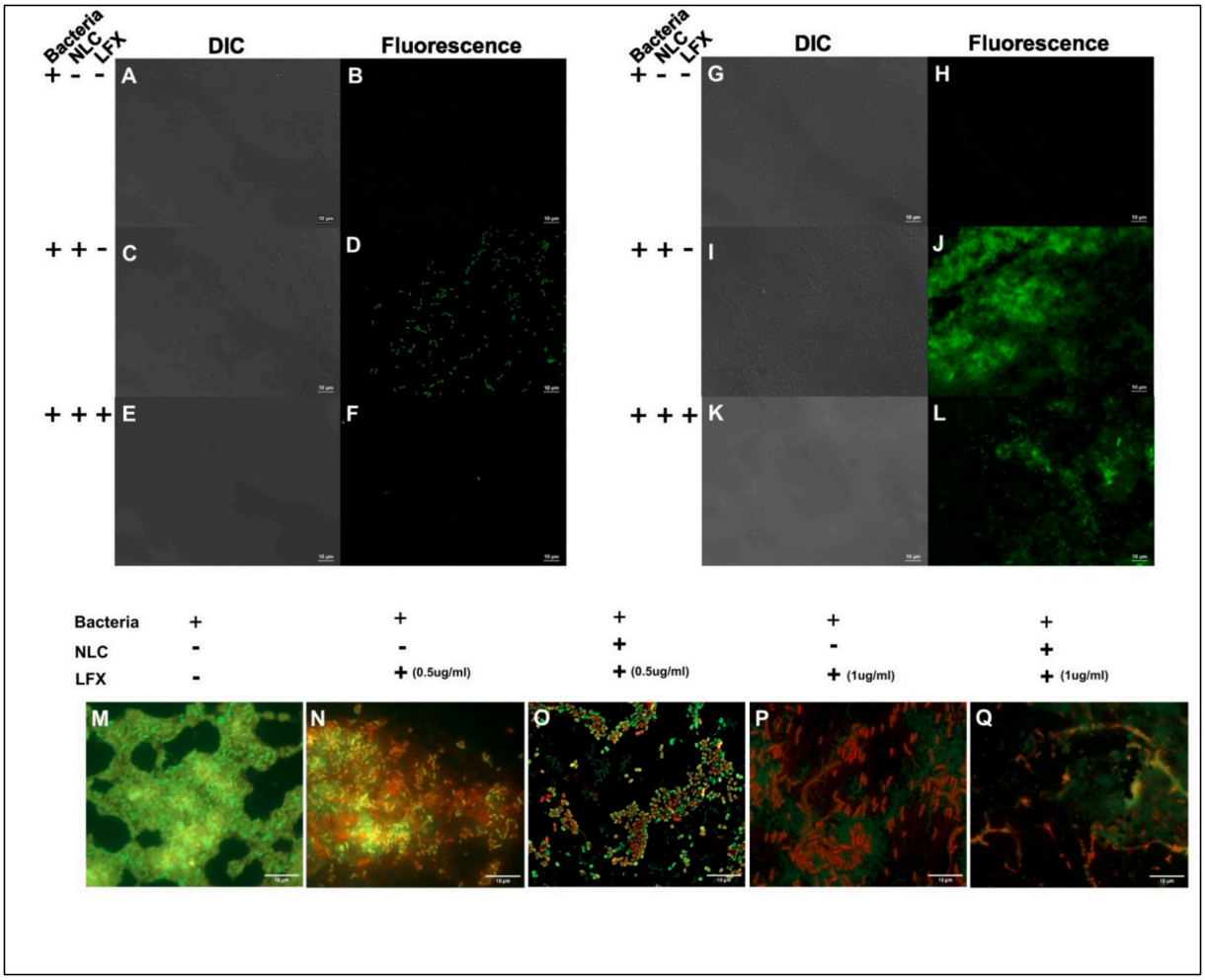

Fig. 7. R-LFX-CO-NLCs are internalised into planktonic bacterial cultures of *P. aeruginosa,* visualised by differential interference contrast (DIC) **A, C, E**, and Rhodamine123 fluorescence **B, D, F** microscopy (630x, oil), deposited on PLL coated coverslips after 4 hours of planktonic growth. **(A-B)**: micrographs of nanoparticle-free media, indicating no fluorescence but bacterial presence. **(C-D)**: Rh-123 loaded CO-NLCs, demonstrating all cells indicate fluorescence. **(E-F)**: R-LFX-CO-NLCs, fewer cells remain but still exhibit fluorescence. R-LFX-CO-NLCs are internalised into bacterial biofilms of *P. aeruginosa* growing on glass. (**G-H)**: micrographs of nanoparticle-free media, indicating no fluorescence **(I-J)**: Rh-123 loaded CO-NLCs, demonstrating all cells indicate fluorescence. **(K-L)**: R-LFX-CO-NLCs, fewer cells remain but still exhibit fluorescence. Live/Dead stained (Syto9/PI) photomicrographs of *P. aeruginosa* biofilms treated with LFX and LFX-CO-NLCs. **(M)** Control biofilm, no treatment, **(N)** LFX 0.5 μg/ml treated biofilm, **(O)** LFX-CO-NLCs 0.5 μg/ml treated biofilm, **(P)** LFX 1.0 μg/ml treated biofilm, **(Q)** LFX-CO-NLCs 1.0 μg/ml treated biofilm. Differences in cell morphology and overall biofilm structure can be observed in O, P & Q compared to M. Scale bars indicate 10μm.

the assays.

3.9.3.3. Nanoparticle internalization assay. To determine whether the loaded NLCs were up taken by bacterial cells or coalesce around them, *P. aeruginosa* exponential and biofilm cultures were challenged with Rhodamine 123 labelled NLCs. The totality of exponentially growing planktonic *P. aeruginosa* cells were green fluorescent, and the fluorescence was evident inside the cells, suggesting that R-LFX-CO-NLCs had been internalized (Fig. 7D). If nanoparticle formulations would have coalesced on the outside of cells, we would have expected the florescence to appear as an outline surrounding the cells. Consistent with observations above, R-LFX-CO-NLCs demonstrated the antibacterial activity of the formulation as well as the absence of fluorescence that would reasonably result from the release of NLCs from dead cells (Fig. 7 E-F). Subsequently, equivalent experiments were undertaken to explore the internalization of NLCs on the biofilm platform. R-LFX-CO-NLCs added to pre-formed biofilms comprehensively stained the biofilm, with the label also inside of the cells, consistent with the observations in planktonic cultures. Interestingly, little biofilm mass was observed after treatment with R-LFX-CO-NLCs, in contrast to the apparent lysis observed in planktonic cells (Fig. 7 K-L). Whilst the biomass was present, it was critical to determine whether these remains consisted of viable cells. Based on the results from Live/Dead staining of biofilm populations treated with LFX-CO-NLCs (1μg/ml) the entirety of the cells was not viable as indicated by the red stain (Fig. 7Q). This would suggest, that even though a portion of biomass remained after LFX-CO-NLCs treatment, this biomass does not represent a viable biofilm, consistent with the findings (Fig. 6).

3.10. In vivo burn wound infection study

Burn wounds infected with *P. aeruginosa* were photographed on 0, 1, 3, 7, 10, and 15 days after treatment to perform a macroscopic study of the wounds and measure the rate of contraction of wound using ImageJ software (Fig. 8A). Compared to untreated control, CO-NLCs hydrogel, and plain LFX gel, treatment with LFX-CO-NLCs hydrogel resulted in a faster reduction in wound size after 15 days of treatment. Quantitative analysis of wound closure revealed a remarkable decrease in wound area (percentage of initial area) in the LFX-CO-NLCs hydrogel treated groups on days 7 (68.10 ± 1.84%), 10 (16.52 ± 1.67%), and 15 (7.34 ± 0.68%) ($P<0.001$), compared to the untreated group where 65.81 ± 4.15% of the wound area remained uncured after 15 days (Fig. 8A). In comparison to the untreated control, the percentage of wound area measured for the

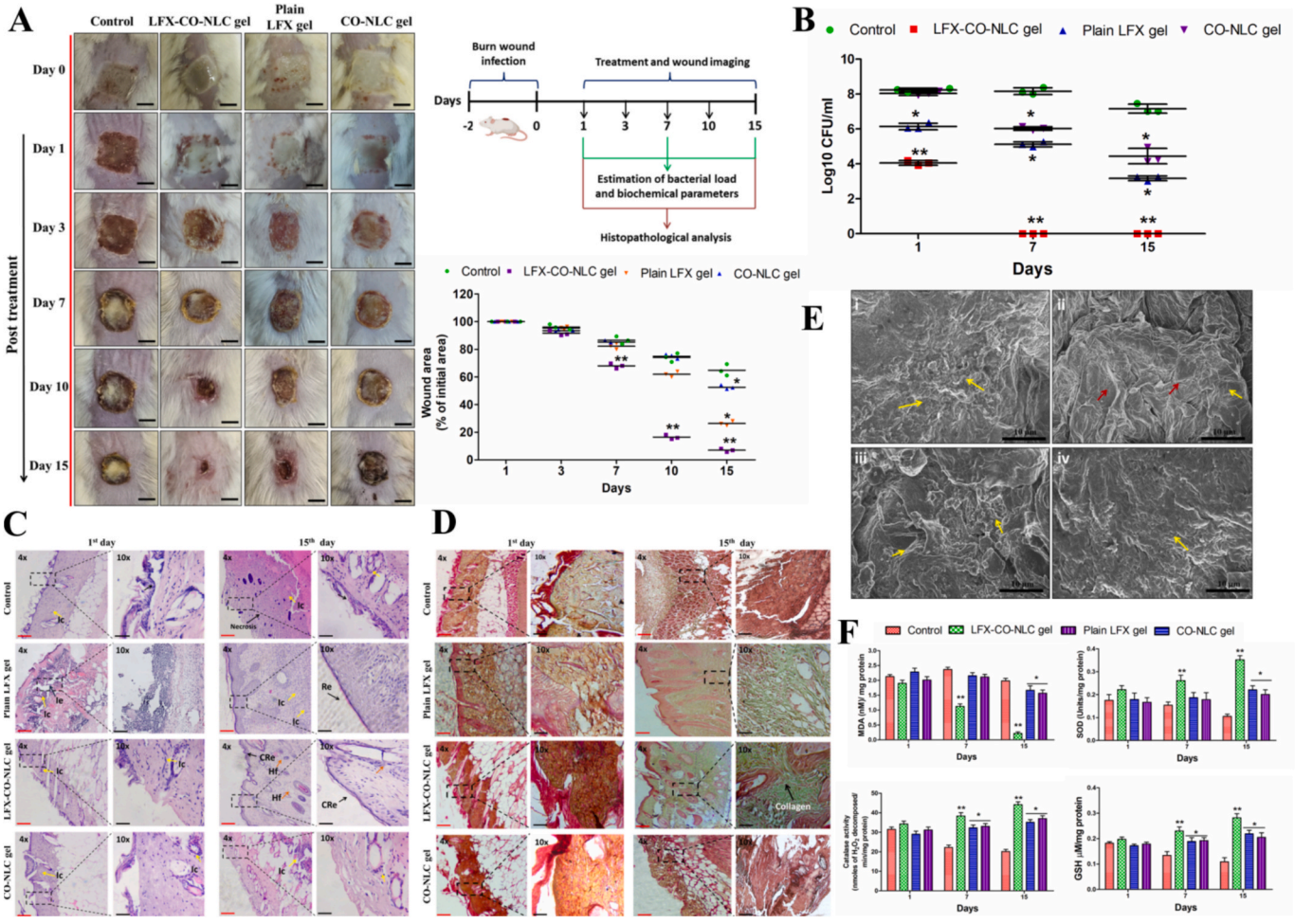

Fig. 8. Accelerated healing of *P. aeruginosa* PAO1 biofilm infected burn wounds by LFX-CO-NLCs hydrogel treatment. **(A)** Representative images of burn wound sites, schematic illustration of the *in vivo* murine burn wound infection and treatment design and graph depicting wound area reduction percentage as compared to initial wound. Scale bar is 5 mm. **(B)** Graph displaying wound bacterial load in $\log_{10}$ CFU/ml. Histological analyses of wound tissues on days 1 and 15 after treatment. **(C)** H&E staining and **(D)** Masson's Trichome staining. Red scale bar = 100 μm; black scale bar = 50 μm. Ic, Re, CRe, Hf and H&E refer to inflammatory cell, re-epithelialization, complete re-epithelialization, and hair follicle, haematoxylin and eosin. **(E)** Characterization of *in vivo P. aeruginosa* PAO1 biofilm using FESEM. (i) untreated control, (ii) LFX-CO-NLCs hydrogel treated, (iii) CO-NLCs gel treated and (iv) LFX gel treated. **(F)** Oxidative stress parameters evaluated during the treatment in wound tissue homogenates. $^{**}P < 0.001$ in comparison to untreated control, LFX gel and CO-NLCs hydrogel. $^{*}P < 0.05$ in comparison to untreated control.

CO-NLCs gel and plain LFX gel at day 15 after treatment were 52.56 ± 1.43% and 24.72 ± 1.52%, respectively ($P<0.05$). As observed from the antibacterial activity experiment, 4-fold decrease in the MIC of LFX against *P. aeruginosa* and antibiofilm activity exerted by LFX-CO-NLCs demonstrates the synergistic effect of LFX and clove oil which led to clearance of bacterial infection from the wound which further led to faster wound healing in comparison to other groups. The biofilm inflicted untreated control group did not heal by itself in 15 days which depicts the inability of the immune system to combat the hyper-inflammatory environment created due to strong biofilm formation by *P. aeruginosa*.

FESEM analysis of excised wound tissue surface after one day of treatment revealed establishment of the biofilm and *in vivo* antibiofilm effect of LFX-CO-NLCs hydrogel. Untreated control exhibited complex biofilm matrix enmeshing *P. aeruginosa* cells within, while LFX-CO-NLCs hydrogel treated group showed biofilm breakdown and visible skin surface which was otherwise hidden underneath the biofilm. This demonstrates translation of *in vitro* antibiofilm effect of LFX-CO-NLCs in *in vivo* environment (Fig. 8E). The antibiofilm effect was also complemented by reduction in wound bacterial load following treatment with LFX-CO-NLCs hydrogel. The extent of the infection was demonstrated by the increase in bacterial count within the untreated control group, which escalated from an initial inoculum of 4 $\log^{10}$ CFU/ml to 8 logs over a span of 15 days, followed by a reduction of approximately 1 log by the conclusion of the treatment period. At the end of treatment, bacterial burden was reduced by ~3.2 logs with CO-NLCs gel and 3.1 logs with plain LFX gel as compared to the control group ($P<0.05$). After one day of treatment with LFX-CO-NLCs hydrogel, bacterial count reduced by 2-fold and complete bacterial clearance was seen after day 7 ($P < 0.001$) which clearly demonstrates its strong antibiofilm and antibacterial efficacy (Fig. 8B).

A histopathological investigation was conducted utilizing H&E and Masson's trichrome staining techniques to monitor and evaluate the alterations in skin tissue at both the initiation and conclusion of the treatment (Fig. 8C-D). Post-burn infliction, loss of skin layers and neutrophil infiltration was observed in all the groups. After completion of the treatment, the untreated control did not heal, and inflammation was still present. CO-NLCs gel treated group showed similar characteristics with presence of infectious exudate and inflammatory cells. Although plain LFX gel group showed full epithelialization there were no indications of hair follicles or any adnexa formation in the dermis that has been regenerated and, inflammatory cells were present in abundance. LFX-CO-NLCs hydrogel treated group demonstrated full re-epithelialization accompanied with regeneration of hair follicles and other glandular formations and minimal inflammation in comparison to other groups. Collagen depletion (MT staining) due to burn injury is evident in all groups in Fig. 8D. On day 15, the control group's skin had not recovered and contained no collagen. The increased intensity of the light green hue from MT staining suggested that LFX-CO-NLCs hydrogel-treated wounds contained more collagen than untreated wounds and collagen was well-organized into fibrils. Collagen deposition was also seen in the plain LFX gel-treated group; however, it was less pronounced than LFX-CO-NLCs hydrogel treated group. No collagen deposition was observed in CO-NLCs gel treated group.

High concentrations of reactive oxygen species, which happen in the early stages of burn injury have been known to initiate oxidative damage. Consequently, a rise in malondialdehyde (MDA) levels is a sign of oxidative damage and lipid peroxidation in epidermal tissues. MDA levels increased a week after wound infection in untreated control group and only dropped mildly at the end of the protocol which gives a picture of severe inflammation prevalent in the wounds (Fig. 8F). Treatment with LFX-CO-NLCs hydrogel led to ~ 2-fold and 4-fold reduction in MDA levels on days 7 and 15, respectively as compared to control ($P<0.01$). LFX-CO-NLCs hydrogel was able to successfully mitigate lipid peroxidation in burn wounds. Superoxide dismutase (SOD) serves as the first line of defense against superoxide anions produced during the inflammatory phase and converts them into hydrogen peroxide. In the control group, SOD levels declined throughout the 15-day period, which may have been caused by an excess of superoxide anions that could not be quenched due to the insufficient amount of SOD generated. However, after 15 days of treatment with LFX-CO-NLCs hydrogel SOD levels increased by ~3-fold ($P < 0.001$) compared to the control, whereas CO-NLCs gel and plain LFX gel exhibited ~2-fold rise ($P < 0.05$).

Two antioxidant enzymes-catalase and reduced glutathione (GSH) come into play to eliminate excess H_2O_2. After 7 days, there was a decrease in catalase levels of the untreated control group which stabilized after 15 days. A considerable increase was noted in the catalase activity on days 7 and 15 for LFX-CO-NLCs hydrogel ($P <0.001$), CO-NLCs gel, and plain LFX gel ($P < 0.05$) as compared to untreated control. The GSH activity for the control and LFX-CO-NLCs hydrogel groups showed a similar pattern. After 15 days, the GSH levels in the LFX-CO-NLCs hydrogel treated group were up to 2.5 times higher (0.282 ± 0.016 μM/mg protein) than in the control group (0.109 ± 0.014) [$P < 0.001$].

4. Discussion

A significant challenge encountered by burn clinics is the risk of bacterial infection within burn wounds, which can result in more serious health conditions, such as sepsis. *P. aeruginosa* is a leading pathogen that commonly colonizes these wounds. It has intrinsic antibiotic resistance, which is associated with the presence of multiple efflux pumps and more importantly its ability to form biofilms which makes the infection severe and difficult to treat. The scarcity of novel antimicrobials, particularly those targeting biofilms, exacerbates the difficulties associated with managing burn wound infections caused by resistant microorganisms. For efficient treatment of wounds which have biofilms, it is pertinent to break down the complex matrix with the aid of an antibiofilm agent to allow antibiotics to access bacterial cells shielded within it. Inhibition of growth of bacterial biofilms by use of an integrated approach by combining a biofilm disruptor with an antibiotic in a nanocarrier would be a powerful strategy to address this challenge.

In this context, our research leveraged the use of NLCs by employing bioactive clove oil as an antibiofilm agent combined with LFX antibiotic for inhibition of bacteria. CO not only provided antibiofilm properties but also contributed as liquid lipid to impart imperfections in the structure of solid lipid Precirol to load higher amounts of LFX in the nanostructure. NLCs loaded with CO can transport antibiofilm components to biofilm surface which will allow LFX to be delivered deep within the matrix by fusion of the NLCs with the bacterial membrane leading to their internalization and subsequent cell death due to LFX mediated DNA damage.

For successful entrapment of LFX within the lipid core of NLCs, selecting lipid with high drug solubility is vital. Lipid solubility of a drug is a crucial parameter for NLCs preparation as it dictates entrapment efficiency which in turn is expected to increase as ability of lipid to solubilize the drug within the core of NLCs increases. Stearic acid demonstrated highest LFX solubility but failed to form stable nanoparticles whereas Precirol® based NLCs formed stable nanosystem with particle size < 200 nm. Precirol® (glyceryl palmitostearate) is a mixture of monoglycerides (8–22%), diglycerides (40–60%) and triglycerides (25–35%) of palmitic and stearic acid. The complex mixture offers less ordered crystal structure which favors high drug loading (Souto et al., 2011). In addition, CO showed high solubilizing capacity for LFX and thus enhanced the drug loading of LFX and formed the liquid part of the lipidic core of NLCs.

An optimal hydrophilic-lipophilic balance (HLB) of the surfactants is essential for the emulsification of the lipid phase in water, from a formulation design standpoint. Lipid phase composed of Precirol® ATO5 has a HLB value of 2, therefore combination of Span 80 (HLB- 4.3) and sodium cholate (HLB- 18) provided stability to the dispersion owing to balanced HLB of the system (Khan et al., 2016). Following

optimization, NLCs with uniform size distribution and stability were obtained as evidenced by low PDI value of 0.227 ± 0.010 and ZP of −43.1 ± 2.22 mV which indicate an electrical barrier impeding the coalescence (Muller et al., 2011). LFX-CO-NLCs remained stable maintaining the particle size, PDI and drug content within acceptable limits over the period of six months. Thermal analysis revealed that LFX was solubilized and integrated within the lipid matrix due to possible conversion into amorphous state.

GC-MS analysis indicated that eugenol, the primary constituent of CO which imparts significant antibacterial and antibiofilm characteristics, remained incorporated within the NLCs. The lipophilicity of eugenol allows it to interact with the lipopolysaccharide layer of bacterial membranes and cause disruption of cellular integrity and subsequent cell death (Devi et al., 2010). Furthermore, eugenol has been shown to possess antibiofilm properties against *P. aeruginosa* biofilms by interfering with quorum sensing mechanism and reducing microbial communication, virulence factor expression, and coordinated biofilm development (Lahiri et al., 2021; Ribeiro et al., 2024).

For enhanced topical application and retention on site, optimized LFX-CO-NLCs were transformed into hydrogel. Adult skin has a pH 4–6, making it mildly acidic due to the presence of acidic keratin, sebum, and eccrine fluids. However, pH of infected burn sites is higher and may range from 6.5 to 10. LFX-CO-NLCs hydrogel with pH of 5.81 would make it compatible with skin and lower the wound pH to promote wound healing. Pseudoplastic behavior and good spreadability of gel promoted its applicability over larger surface area. Based on *in vitro* release study, LFX-CO-NLCs hydrogel showed initial burst release of ~40% of drug in 1 h, followed by sustained release over a period of 8 h showing two-phase release. The initial burst release would deliver a high concentration of antibiotics to effectively inhibit biofilm formation, while a sustained release exceeding the MIC would facilitate the elimination of any remaining cells (Pastor et al., 2014).

Cellular compatibility and safety are an essential aspect for topical administration of the developed LFX-CO-NLCs for the treatment of wound infection. Cell culture studies were carried out to determine the safety, uptake and *in vitro* wound healing effects of LFX-CO-NLCs. Cell viability levels above 70% are regarded as non-cytotoxic in comparison to untreated control cells (Bauer, 2007:). The biocompatibility of LFX-CO-NLCs was demonstrated in two skin cell lines, epithelial (NHEK) and fibroblast (HDF-a) with cell viability >80% in both the cell lines. LFX-CO-NLCs showed concentration dependent uptake in NHEK and HDF-a cells and showed localization in cytoplasm of HDF-a cells. LFX-CO-NLCs were up taken majorly by macropinocytosis and clathrin-mediated endocytosis. Macropinocytosis is an actin dependent non-specific uptake process that results in the formation of macropinosomes, which are large endocytic vacuoles. Actin filaments are known to be depolymerized by cytochalasin B, which prevents membrane ruffles formation and cell uptake. Additionally, incubation with hypertonic growth media (0.45 M sucrose) showed reduction in cellular uptake which could be attributed to suppression of clathrin, an essential internalization route for endocytosis, by inhibiting the formation of clathrin-coated pits and the subsequent scission from the plasma membrane (Zwain et al., 2023; Khurana et al., 2018).

In cell cycle analysis, a reduction in the percentage of G0/G1 phase cells and an increment in the population of G2/M phase cells were noted in HDF-a cells treated with LFX-CO-NLCs. This observation suggests that the enhanced proliferation rate is attributable to a higher rate of transition into the S phase, which implies a greater number of cells undergoing mitosis. As seen in cell viability and cell cycle analysis, LFX-CO-NLCs did not show any cellular toxicity and promoted cell proliferation. Eugenol, recognized as the predominant compound in CO has been reported to enhance cell proliferation and facilitate the process of wound healing. (Banerjee et al., 2020; Sisakhtnezhad et al., 2018). It could be hypothesized that uptake of NLCs laden with CO into the cytoplasm promoted wound healing. Indeed, one of the mechanisms linked with bioactivity augmentation is the internalization of the active substance into the cell cytoplasm, as has been previously documented (Shah et al., 2011). Further *in vitro* scratch assay in HDF-a cells demonstrated enhanced wound closure which complemented the results obtained in cell cycle analysis. This could be attributed to the wound healing characteristic of the CO in the lipid nanocarriers. Saha et al. have also shown that CO loaded cryogels promote fibroblast migration and lead to rapid closure of *in vitro* scratch wounds (Saha and Tayalia, 2022).

In vitro agar well diffusion and MIC studies demonstrated co-loading of LFX and CO into lipid nanocarriers enhanced its antibacterial activity which could be attributed to synergistic effect of LFX and CO and enhanced penetration of nano-antibiotic into the bacterial cells owing to similarity of lipid nanoparticles with bacterial cell membrane which facilitates fusion with the cell membrane (Mamun et al., 2021). Antibiofilm studies on *P. aeruginosa* biofilm using CV assay showed the biofilm disruptor properties of LFX-CO-NLCs and significant reduction in bacterial count as compared to LFX solution. The enhanced antibacterial effect of antibiotic-loaded NLCs could be due to (i) coalescence of NLCs in the vicinity of the bacterial cells and local external release of the drug, or (ii) penetration of NLCs in the cell envelopes and delivery in the cytosol. To determine whether the loaded NLCs were up taken by bacterial cells or coalesce around them, *P. aeruginosa* exponential and biofilm cultures were challenged with Rh123 labelled NLCs. The R-CO-NLCs were up taken by bacterial cells in planktonic form while treatment with R-LFX-CO-NLCs led to uptake and eventual cell death of bacteria. Biofilm treated with R-LFX-CO-NLCs showed penetration of nanoparticles through the biofilm into the bacterial cells as well as subsequent disruption of biofilm architecture. The negative charge of NLCs would have contributed to the biofilm penetration as it has been reported that lipid nanoparticles with neutral/negatively charged surface charge penetrate the biofilm better (Alhariri et al., 2017; Zou et al., 2022). Live/dead staining confirmed that biofilm remanent left after treatment with R-LFX-CO-NLCs did not constitute a viable biofilm. The NLCs are composed of solid and liquid lipids. In our work, Precirol (solid lipid) and clove oil (liquid lipid) are used in equal ratios (1:1). Therefore, in essence, clove oil forms the structure of the NLCs and will be in first contact with the biofilm. Upon coming in contact with the biofilm, the components of clove oil will exert its antibiofilm effect, followed by the release of the drug levofloxacin to have bactericidal effect. Our results are in line with those obtained by Sans-Serramitjana et al. where they demonstrated enhanced penetration and antibiofilm effect of colistin loaded NLCs in *P. aeruginosa* biofilms (Sans-Serramitjana et al., 2017).

Finally, the efficacy of LFX-CO-NLCs was evaluated in *P. aeruginosa* biofilm inflicted burn wound infection in mice. *In-vitro* antibiofilm, antibacterial and wound healing capabilities demonstrated by LFX-CO-NLCs were confirmed in the *in-vivo* model which showed complete clearance of infection and healing of the burn wound. Burn lesions are notorious for being colonised by opportunistic microorganisms such as *Pseudomonas aeruginosa* and *Staphylococcus aureus*. The propensity of these pathogens to establish biofilms is a key factor in their pathogenic success and significantly complicates the management of burn wounds (Percival et al., 2015). As confirmed by FESEM analysis, biofilm formation was observed in burn wounds after two days of the induction of infection. Daily treatment with LFX-CO-NLCs hydrogel for 15 days led to complete wound healing and eradication of *P. aeruginosa* infection was observed within seven days of treatment. This could be attributed to presence of CO in the NLCs which disrupted the biofilm allowing LFX to kill the bacteria and clear the infection while clove oil due to its anti-inflammatory and wound healing activities facilitated the wound healing. Perteghella et al. also demonstrated healing of burn wounds in mice after treatment with CO containing nanoemulsion (Perteghella et al., 2023). Therefore, use of NLCs to deliver an antibiotic and an essential oil as an antibiofilm agent can prove to be a promising strategy for the treatment of chronically infected wounds.

5. Conclusion

The present study entails successful fabrication of NLCs co-loaded with CO and LFX for the treatment of burn wounds infected with *P. aeruginosa* biofilm. The optimized nano-system was stable over a span of 6 months in both liquid and hydrogel form. *In vitro* release studies demonstrated a dual-controlled delivery platform, where drug release is regulated by both the lipid matrix of the NLCs and the hydrogel network. A bi-phasic release pattern would provide high initial LFX concentration to have immediate antibacterial effect followed by sustained release for prolonged effect. Future investigations will also include release kinetics of clove oil components to understand their effect on biofilm disruption.

LFX-CO-NLCs were effectively internalized by planktonic bacteria as well as penetrated through the *P. aeruginosa* biofilm leading to its subsequent destruction. *In-vitro* study in skin cell lines ratify the cyto-compatibility and wound healing potential of LFX-CO-NLCs. LFX-CO-NLCs are clearly more efficient than LFX in eliminating *P. aeruginosa* biofilm *in vitro* and from the burn wounds *in vivo* and promote wound healing. This could be attributed to nano-encapsulated CO and LFX in dual functional NLCs to access both peripheral and deeper neighborhoods of biofilm, inhibit the infection causing bacteria and stimulate tissue regeneration and wound healing process. Thus, using an integrated approach with an antibiotic loaded along with a biofilm disruptor in a nanocarrier, demonstrates the potential of LFX-CO-NLCs hydrogel to enhance drug therapy not only for burn wound infections but could also be extended to chronic wounds challenged with bacterial biofilm as a promising strategy for biofilm-targeted wound management. This novel approach also has the potential to save antibiotics that would otherwise be in oblivion due to AMR. As a bonus, the alarming rise of antibiotic-resistant bacterial strains can be reduced, making up for the dearth of novel compounds.

Funding

Karan Razdan, the first author, recognizes the financial support provided by the Department of Science and Technology, India [DST INSPIRE SRF (IF170172)] and the first author and corresponding author KKS acknowledge the financial support provided by Commonwealth Scholarship Commission, UK (INCN-2019-380) for carrying out research work at University of Lancashire, UK.

CRediT authorship contribution statement

Karan Razdan: Writing – original draft, Methodology, Investigation, Formal analysis, Data curation. **Matthew Allott:** Methodology, Investigation. **Shashi Kanta:** Investigation. **Ekta Chaudhary:** Investigation. **Deepak Kumar Rahi:** Methodology, Resources. **Seema Kumari:** Investigation. **Tamara Zwain:** Investigation. **Jorge Garcia Lara:** Supervision, Methodology. **Vivek Ranjan Sinha:** Supervision, Resources. **Kamalinder K. Singh:** Writing – review & editing, Visualization, Supervision, Resources, Project administration, Methodology, Funding acquisition, Formal analysis, Conceptualization.

Declaration of competing interest

The authors declare that they have no known competing financial interests or personal relationships that could have appeared to influence the work reported in this paper.

Appendix A. Supplementary data

Supplementary data to this article can be found online at https://doi.org/10.1016/j.ijpharm.2026.126885.

Data availability

Data will be made available on request.

References

Alhariri, M., et al., 2017. Efficacy of neutral and negatively charged liposome-loaded gentamicin on planktonic bacteria and biofilm communities. Int. J. Nanomed. 12, 6949–6961.
Banerjee, K., Madhyastha, H., Sandur, R., NT M, Thiagarajan, P., 2020. Anti-inflammatory and wound healing potential of a clove oil emulsion. Colloids Surf. B Biointerfaces 193, 111102.
Bauer, S.R., 2007. Stem cell-based products in medicine: FDA regulatory considerations. Handbook of Stem Cells 805.
Bazargani, M.M., Rohloff, J., 2016. Antibiofilm activity of essential oils and plant extracts against Staphylococcus aureus and Escherichia coli biofilms. Food Control 61, 156–164.
Beraldo-Araújo, V.L., et al., 2022. Levofloxacin in nanostructured lipid carriers: preformulation and critical process parameters for a highly incorporated formulation. Int. J. Pharm. 626, 122193.
Budzyńska, A., Wieckowska-Szakiel, M., Sadowska, B., Kalemba, D., Rozalska, B., 2011. Antibiofilm activity of selected plant essential oils and their major components. Pol. J. Microbiol. 60 (1), 35–41.
Ciofu, O., Moser, C., Jensen, P.Ø., Høiby, N., 2022. Tolerance and resistance of microbial biofilms. Nat. Rev. Microbiol. 20 (10), 621–635.
Das, S., Ng, W.K., Tan, R.B.H., 2012. Are nanostructured lipid carriers (NLCs) better than solid lipid nanoparticles (SLNs)? Development, characterization and comparative evaluation of clotrimazole-loaded lipid nanoparticles. Int. J. Pharm. 364 (1), 45–53.
Devi, K.P., Nisha, S.A., Sakthivel, R., Pandian, S.K., 2010. Eugenol (an essential oil of clove) acts as an antibacterial agent against Salmonella typhi by disrupting the cellular membrane. J. Ethnopharmacol. 130 (1), 107.
Diab, R., Khameneh, B., Joubert, O., Duval, R., 2015. Insights in nanoparticle-bacterium interactions: new frontiers to bypass bacterial resistance to antibiotics. Curr. Pharm. Des. 21 (28), 4095–4105.
Dolatabadi, S., Karimi, M., Nasirizadeh, S., Hatamipour, M., Golmohammadzadeh, S., Jaafari, M.R., 2021. Preparation, characterization and in vivo pharmacokinetic evaluation of curcuminoids-loaded solid lipid nanoparticles (SLNs) and nanostructured lipid carriers (NLCs). J. Drug Deliv. Sci. Tech. 62, 102352.
Elbestawy, M.K., El-Sherbiny, G.M., Moghannem, S.A., 2023. Antibacterial, antibiofilm and anti-inflammatory activities of eugenol clove essential oil against resistant Helicobacter pylori. Molecules 28 (6), 2448.
Elmowafy, M., Al-Sanea, M.M., 2021. Nanostructured lipid carriers (NLCs) as drug delivery platform: advances in formulation and delivery strategies. Saudi Pharm J. 29 (9), 999–1012.
Ghasemian, S., et al., 2023. Molecular characterizations of antibiotic resistance, biofilm formation, and virulence determinants of Pseudomonas aeruginosa isolated from burn wound infection. J. Clin. Lab. Anal. 37 (4), e24850.
Ghodrati, M., Farahpour, M.R., Hamishehkar, H., 2019. Encapsulation of Peppermint essential oil in nanostructured lipid carriers: in-vitro antibacterial activity and accelerative effect on infected wound healing. Colloids Surf. A Physicochem. Eng. Asp. 564, 161–169.
Giordano, P., Weber, K., Gesin, G., Kubert, J., 2007. Skin and skin structure infections: treatment with newer generation fluoroquinolones. Ther. Clin. Risk Manag. 3 (2), 309–317.
Gorman, E.M., Samas, B., Munson, E.J., 2012. Understanding the dehydration of levofloxacin hemihydrate. J. Pharm. Sci. 101 (9), 3319–3330.
Gupta, P., Chhibber, S., Harjai, K., 2015. Efficacy of purified lactonase and ciprofloxacin in preventing systemic spread of Pseudomonas aeruginosa in murine burn wound model. Burns 41 (1), 153–162.
Hameed, M., et al., 2021. Formulation and evaluation of a clove oil-encapsulated nanofiber formulation for effective wound-healing. Molecules 26 (9), 2491.
Hemalatha, R., Nivetha, P., Mohanapriya, C., Sharmila, G., Muthukumaran, C., Gopinath, M., 2016. Phytochemical composition, GC-MS analysis, in vitro antioxidant and antibacterial potential of clove flower bud (Eugenia caryophyllus) methanolic extract. J. Food Sci. Tech. 53, 1189–1198.
Henostroza, M.A., et al., 2022. Antibiotic-loaded lipid-based nanocarrier: a promising strategy to overcome bacterial infection. Int. J. Pharm. 621, 121782.
Khan, S., Shaharyar, M., Fazil, M., Baboota, S., Ali, J., 2016. Tacrolimus-loaded nanostructured lipid carriers for oral delivery–Optimization of production and characterization. Eur. J. Pharm. Biopharm. 108, 277.
Khurana, R.K., et al., 2018. Clathrin-mediated endocytic uptake of PUFA enriched self-nanoemulsifying lipidic systems (SNELS) of an anticancer drug against triple negative cancer and DMBA induced preclinical tumor model. Mat. Sci. Eng.: C. 91, 645–658.
Koch, H.R., Kulus, S.C., Roessler, M., Ropo, A., Geldsetzer, K., 2005. Corneal penetration of fluoroquinolones: aqueous humor concentrations after topical application of levofloxacin 0.5% and ofloxacin 0.3% eyedrops. J. Cataract Refract Surg 31 (7), 1377–1385.
Lahiri, D., Nag, M., Dutta, B., Dey, S., Mukherjee, D., Joshi, S.J., Ray, R.R., 2021. Antibiofilm and anti-quorum sensing activities of eugenol and linalool from Ocimum tenuiflorum against Pseudomonas aeruginosa biofilm. J. Appl. Microbiol. 131 (6), 2821–2837.
Liang, C.C., Park, A.Y., Guan, J.L., 2007. In vitro scratch assay: a convenient and inexpensive method for analysis of cell migration in vitro. Nat. Protoc. 2 (2), 329–333.
Liu, H.H., 2010. Safety profile of the fluoroquinolones: focus on levofloxacin. Drug Saf. 33, 353–369.
Mamun, M.M., Sorinolu, A.J., Munir, M., Vejerano, E.P., 2021. Nanoantibiotics: functions and properties at the nanoscale to combat antibiotic resistance. Front. Chem. 9, 687660.

Manzoor, A., Asif, M., Khalid, S.H., Ullah Khan, I., Asghar, S., 2023. Nanosizing of lavender, basil, and clove essential oils into microemulsions for enhanced antioxidant potential and antibacterial and antibiofilm activities. ACS Omega 8 (43), 40600–40612.
Martins, S., Costa-Lima, S., Carneiro, T., Cordeiro-da-Silva, A., Souto, E.B., Ferreira, D.C., 2012. Solid lipid nanoparticles as intracellular drug transporters: an investigation of the uptake mechanism and pathway. Int. J. Pharm. 430 (1–2), 216–227.
Müller, R.H., Radtke, M., Wissing, S.A., 2002. Nanostructured lipid matrices for improved microencapsulation of drugs. Int. J. Pharm. 242 (1–2), 121–128.
Muller, H.R., Shegokar, R., Keck, M.C., 2011. 20 years of lipid nanoparticles (SLN & NLC): present state of development & industrial applications. Curr. Drug. Discov. Tech. 8 (3), 207–227.
Pastor, M., et al., 2014. Sodium colistimethate loaded lipid nanocarriers for the treatment of Pseudomonas aeruginosa infections associated with cystic fibrosis. Int. J. Pharm. 477 (1–2), 485–494.
Pásztor, N., Rédai, E., Szabó, Z.I., Sipos, E., 2017. Preparation and characterization of levofloxacin-loaded nanofibers as potential wound dressings. Acta Med. Marisiensis. 63 (2), 66–69.
Percival, S.L., McCarty, S.M., Lipsky, B., 2015. Biofilms and wounds: an overview of the evidence. Adv. Wound Care 4 (7), 373–381.
Perteghella, S., et al., 2023. Nanoemulsions of clove oil stabilized with chitosan oleate-antioxidant and wound-healing activity. Antioxidants 12 (2), 273.
Podolsky, S.H., 2018. The evolving response to antibiotic resistance (1945–2018). Palgrave Commun. 4 (1).
Pople, P.V., Singh, K.K., 2006. Development and evaluation of topical formulation containing solid lipid nanoparticles of vitamin A. AAPS PharmSciTech 7 (4), 91. https://doi.org/10.1208/pt070491.
Razdan, K., Gondil, V.S., Chhibber, S., Singh, K.K., Sinha, V.R., 2022. Levofloxacin loaded clove essential oil nanoscale emulsion as an efficient system against Pseudomonas aeruginosa biofilm. J. Drug Deliv. Sci. Tech. 68, 103039.
Razdan, K., Garcia-Lara, J., Sinha, V.R., Singh, K.K., 2022. Pharmaceutical strategies for the treatment of bacterial biofilms in chronic wounds. Drug Discov. Today 27 (8), 2137–2150.
Razdan, K., Kanta, S., Chaudhary, E., Kumari, S., Rahi, D.K., Yadav, A.K., Sinha, V.R., 2023. Levofloxacin loaded clove oil nanoscale emulgel promotes wound healing in Pseudomonas aeruginosa biofilm infected burn wound in mice. Colloids Surf. B Biointerfaces 222, 113113.
Ribeiro, T.A., Dos Santos, G.A., Dos Santos, C.T., Soares, D.C., Saraiva, M.F., Leal, D.H., Sachs, D., 2024. Eugenol as a promising antibiofilm and anti-quorum sensing agent: a systematic review. Microb. Pathog. 196, 106937.
Saha, L., et al., 2023. Neuroprotective effect of berberine nanoparticles against seizures in pentylenetetrazole induced kindling model of epileptogenesis: role of anti-oxidative, anti-inflammatory, and anti-apoptotic mechanisms. Neurochem. Res. 48 (10), 3055–3072.
Saha, R., Tayalia, P., 2022. Clove oil-incorporated antibacterial gelatin–chitosan cryogels for tissue engineering: an in vitro study. ACS Biomat. Sci. Eng. 8 (8), 3557–3567.
Sakellari, G.I., Zafeiri, I., Batchelor, H., Spyropoulos, F., 2021. Formulation design, production and characterisation of solid lipid nanoparticles (SLN) and nanostructured lipid carriers (NLC) for the encapsulation of a model hydrophobic active. Food Hydrocoll Health. 1, 100024.
Sans-Serramitjana, E., Jorba, M., Pedraz, J.L., Vinuesa, T., Viñas, M., 2017. Determination of the spatiotemporal dependence of Pseudomonas aeruginosa biofilm viability after treatment with NLC-colistin. Int. J. Nanomed. 4409–4413.
Sathe, N., Beech, P., Croft, L., Suphioglu, C., Kapat, A., Athan, E., 2023. Pseudomonas aeruginosa: infections and novel approaches to treatment "knowing the enemy" the threat of Pseudomonas aeruginosa and exploring novel approaches to treatment. Infect. Med. 2 (3), 178–194.
Sepahvand, S., Amiri, S., Radi, M., Amiri, M.J., 2022. Effect of thymol and nanostructured lipid carriers (NLCs) incorporated with thymol as antimicrobial agents in sausage. Sustainability 14 (4), 1973.
Shah, D.A., Kwon, S.J., Bale, S.S., Banerjee, A., Dordick, J.S., Kane, R.S., 2011. Regulation of stem cell signaling by nanoparticle-mediated intracellular protein delivery. Biomaterials 32 (12), 3210–3219.
Siafaka, P.I., Zisi, A.P., Exindari, M.K., Karantas, I.D., Bikiaris, D.N., 2016. Porous dressings of modified chitosan with poly (2-hydroxyethyl acrylate) for topical wound delivery of levofloxacin. Carbohydr. Polym. 143, 90–99.
Silva, E., Barreiros, L., Segundo, M.A., Lima, S.A., Reis, S., 2017. Cellular interactions of a lipid-based nanocarrier model with human keratinocytes: Unravelling transport mechanisms. Acta Biomater. 53, 439.
Sisakhtnezhad, S., Heidari, M., Bidmeshkipour, A., 2018. Eugenol enhances proliferation and migration of mouse bone marrow-derived mesenchymal stem cells in vitro. Environ. Toxicol. Pharmacol. 57, 166–174.
Souto, E.B., Doktorovova, S., Boonme, P., 2011. Lipid-based colloidal systems (nanoparticles, microemulsions) for drug delivery to the skin: materials and end-product formulations. J. Drug Deliv. Sci. Tech. 21 (1), 43–54.
Suarez-Arnedo, A., Figueroa, F.T., Clavijo, C., Arbeláez, P., Cruz, J.C., Muñoz-Camargo, C., 2020. An image J plugin for the high throughput image analysis of in vitro scratch wound healing assays. PLoS One 15 (7), e0232565.
Teng, Z., et al., 2019. Preparation and characterization of nimodipine-loaded nanostructured lipid systems for enhanced solubility and bioavailability. Int. J. Nanomed. 119–133.
Üner, M., 2006. Preparation, characterization and physico-chemical properties of solid lipid nanoparticles (SLN) and nanostructured lipid carriers (NLC): their benefits as colloidal drug carrier systems. Die pharmazie-an Int. J. Pharm. Sci. 61 (5), 375–386.
Uruén, C., Chopo-Escuin, G., Tommassen, J., Mainar-Jaime, R.C., Arenas, J., 2020. Biofilms as promoters of bacterial antibiotic resistance and tolerance. Antibiotics 10 (1), 3.
Valizadeh, A., Shirzad, M., Pourmand, M.R., Farahmandfar, M., Sereshti, H., Amani, A., 2021. Levofloxacin nanoemulsion gel has a powerful healing effect on infected wound in streptozotocin-induced diabetic rats. Drug Deliv. Transl. Res. 11, 292–304.
Vestby, L.K., Grønseth, T., Simm, R., Nesse, L.L., 2020. Bacterial biofilm and its role in the pathogenesis of disease. Antibiotics 9 (2), 59.
Zou, et al., 2022. Antibiotics-free nanoparticles eradicate Helicobacter pylori biofilms and intracellular bacteria. J. Control. Release 348, 370–385.
Zwain, T., Alder, J.E., Sabagh, B., Shaw, A., Burrow, A.J., Singh, K.K., 2021. Tailoring functional nanostructured lipid carriers for glioblastoma treatment with enhanced permeability through in-vitro 3D BBB/BBTB models. Mat. Sci. Eng.: C. 121, 111774.
Zwain, T., Alder, J.E., Zwayen, S., Shaw, A., Burrow, A.J., Singh, K.K., 2023. Overcoming biological barriers BBB/BBTB by designing PUFA functionalised lipid-based nanocarriers for glioblastoma targeted therapy. Biomater. Adv. 155, 213660.